

Leveraging an Open Science Drug Discovery Model to Develop CNS-Penetrant ALK2 Inhibitors for the Treatment of Diffuse Intrinsic Pontine Glioma

David Smil,* Jong Fu Wong, Eleanor P. Williams, Roslin J. Adamson, Alison Howarth, David A. McLeod, Ahmed Mamai, Soyoung Kim, Brian J. Wilson, Taira Kiyota, Ahmed Aman, Julie Owen, Gennady Poda, Kurumi Y. Horiuchi, Ekaterina Kuznetsova, Haiching Ma, J. Nicole Hamblin, Sue Cramp, Owen G. Roberts, Aled M. Edwards, David Uehling, Rima Al-awar, Alex N. Bullock, Jeff A. O'Meara, and Methvin B. Isaac*

Cite This: *J. Med. Chem.* 2020, 63, 10061–10085

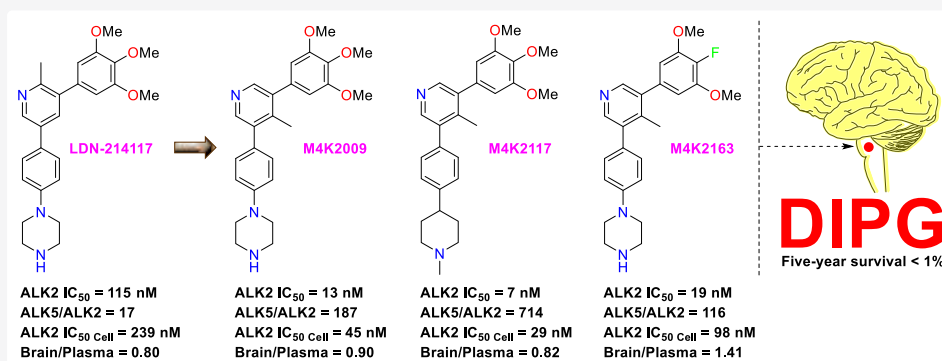
Read Online

ACCESS |

Metrics & More

Article Recommendations

Supporting Information



ABSTRACT: There are currently no effective chemotherapeutic drugs approved for the treatment of diffuse intrinsic pontine glioma (DIPG), an aggressive pediatric cancer resident in the pons region of the brainstem. Radiation therapy is beneficial but not curative, with the condition being uniformly fatal. Analysis of the genomic landscape surrounding DIPG has revealed that activin receptor-like kinase-2 (ALK2) constitutes a potential target for therapeutic intervention given its dysregulation in the disease. We adopted an open science approach to develop a series of potent, selective, orally bioavailable, and brain-penetrant ALK2 inhibitors based on the lead compound LDN-214117. Modest structural changes to the C-3, C-4, and C-5 position substituents of the core pyridine ring afforded compounds M4K2009, M4K2117, and M4K2163, each with a superior potency, selectivity, and/or blood–brain barrier (BBB) penetration profile. Robust *in vivo* pharmacokinetic (PK) properties and tolerability mark these inhibitors as advanced preclinical compounds suitable for further development and evaluation in orthotopic models of DIPG.

INTRODUCTION

Pediatric central nervous system (CNS) tumors constitute a heterogeneous group of diseases, and patient survival rates vary greatly among tumor subtypes.¹ Diffuse intrinsic pontine glioma (DIPG), a grade IV tumor originating in glial tissue of the pons and typically affecting children between 5 and 7 years of age,^{2,3} is highly infiltrative with a 5-year relative survival rate of less than 1%.⁴ While accounting for 10% of all pediatric brain tumors, a median survival of just 9–12 months means that the prognosis for children with DIPG is particularly poor relative to those with other brainstem cancers.⁵ Given that the pons contains cranial nerve nuclei and nuclei critical for life-sustaining functions such as respiration and sleep, damage by the tumor or treatment has potentially severe repercussions.⁶ Sensitivity of the affected pons region renders it unsuitable for surgical resection, so the current

standard of care is limited to focal radiation therapy providing only limited and temporary benefit for patient survival.⁷ Chemotherapeutic agents have also met with little success in prolonging patient survival,^{4,6} in part because CNS drug exposure is limited by the endothelial tight junctions and elevated expression levels of efflux transporters at the blood–brain barrier (BBB), making it difficult to reach therapeutically relevant drug concentrations at lesion sites.⁸ A number of brain-

Received: July 10, 2020

Published: August 11, 2020



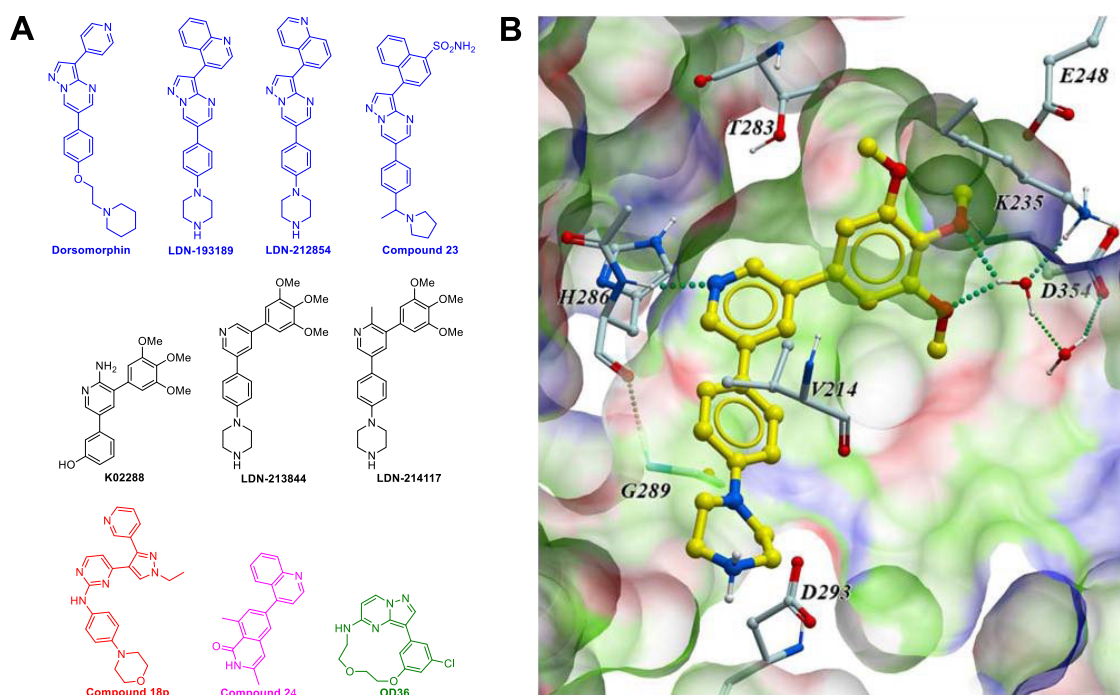


Figure 1. (A) Reported ALK2 inhibitors based on pyrazolo[1,5-*a*]pyrimidine (blue), 3,5-diphenylpyridine (black), bis-heteroaryl pyrazole (red), quinazolinone (magenta), and macrocyclic (green) scaffolds. (B) Cocrystal structure of prototypic 3,5-diphenylpyridine inhibitor LDN-213844 (yellow) with ALK2 (PDB code 4BGG).³⁷

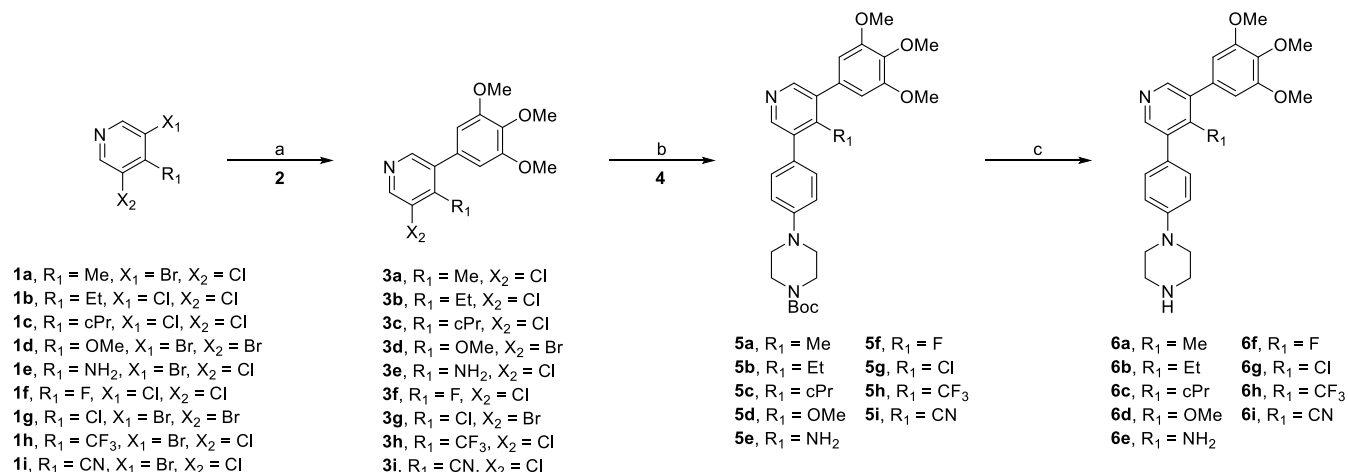
penetrant chemotherapeutic agents such as temozolomide and vincristine have been explored as complements to radiotherapy, but no significant improvement in outcomes has been observed.^{9,10}

The advent of modern stereotactic procedures to safely biopsy DIPG tumors¹¹ has opened new avenues for molecular characterization and overturned old orthodoxies relating to the classification and treatment of both adult and childhood gliomas as similar tumors.¹² In contrast to the *IDH1/2*, *BRAF*, or *FGFR* oncogenic driver mutations found in adult gliomas, mutations in histone and developmental signaling proteins are characteristic of DIPG.^{13,14} Somatic missense mutations in the bone morphogenetic protein (BMP) type I receptor *ACVR1* gene encoding activin receptor-like kinase-2 (ALK2), one of the seven (ALK1–7) type I receptors in the transforming growth factor β (TGF β)/BMP signaling pathway, have been reported in approximately 33% of children with DIPG.^{2,3} The *ACVR1* gene, widely expressed in a variety of tissues including bone, cartilage, heart, CNS, and the reproductive system, is located in chromosome 2q23-q24 and encodes for the 509 amino acid protein.¹⁵ Although rare in other human cancers, similar *ACVR1* mutations are found in individuals with fibrodysplasia ossificans progressiva (FOP), a monogenic developmental disorder whose primary features are skeletal abnormalities and heterotopic ossification.^{16–18} In DIPG, mutant *ACVR1* is ubiquitous throughout the tumors and strongly associated with K27M mutations in *HIST1H3B*, suggesting a partnership with H3K27M mutations during clonal evolution.¹⁹

Comprising an extracellular ligand binding domain and an intracellular serine/threonine (Ser/Thr) kinase domain, ALK2 functions as a transmembrane receptor.²⁰ When BMP ligands bind to a complex of ALK2 and type II BMP receptors, the resultant activation of ALK2 by transphosphorylation of its juxtamembrane glycine–serine (GS)-rich domain promotes the recruitment and phosphorylation of downstream transcription

factors SMAD1/5/8 by ALK2 and subsequent induction of BMP-response genes such as *ID1-3* (known mediators of gliomagenesis).^{21–23} Heterozygous somatic nonsynonymous missense gain-of-function mutations present exclusively in the cytoplasmic GS (20% R206H and 2% Q207E) and Ser/Thr kinase domains (13% R258G, 24% G328E, 28% G328V, 4% G328W, and 9% G356D)² of ALK2 not only result in hypersensitivity to canonical BMP ligands but also induce responsiveness to activin ligands.^{24,25} Each *ACVR1* mutant was found to increase basal canonical BMP pathway signaling when overexpressed in cultured mouse primary astrocytes, suggesting a role for these mutations during neurodevelopment.² Although mutant ALK2 alone is not sufficient to drive tumor formation (*i.e.*, FOP patients with somatic ALK2 mutations do not develop DIPG) and the mechanistic role of ALK2 in DIPG pathogenesis has not yet been fully elucidated,^{2,26} significant cooperation between mutant ALK2 and the oncohistone H3.1K27M has been demonstrated in neurospheres, with a strong influence of ALK2 on gliomagenesis (initiation, proliferation, and survival) observed.²⁷ In H3.3K27M *ACVR1*^{R206H} HSJD-DIPG-007 cells, shRNA knockdown of *ACVR1* not only caused reduction in cell viability but also resulted in increased apoptotic cell death. While mutated histone H3 is not directly druggable, ALK2 is a classical protein kinase constituting a suitable target for a drug discovery program.

Following the discovery that an adenosine monophosphate (AMP)-activated kinase inhibitor, Dorsomorphin, could block BMP signaling through SMAD1/5/8 phosphorylation,²⁸ a number of related inhibitors centered around the pyrazolo[1,5-*a*]pyrimidine chemotype were reported (Figure 1A).²⁹ Inhibitors of ALK2 such as LDN-193189³⁰ and LDN-212854^{31,32} showed efficacy in FOP mouse models³³ although their activity against a number of kinase off-targets³⁴ and dose-limiting toxicity (a 10% body weight loss in animal models)³⁵ ultimately constrain their clinical utility. Biochemical screening

Scheme 1. Synthesis of Compounds 6a–i⁴⁴

⁴⁴Reagents and conditions: (a) 3,4,5-trimethoxyphenylboronic acid (**2**), Pd(dppf)Cl₂·dichloromethane (DCM), Na₂CO₃, *N,N*-dimethylformamide (DMF)/H₂O, 100 °C, 16 h for **1a**, **1d–e**, **1g**, **1i** and XPhos Pd G2, K₃PO₄, butanol/H₂O, 100 °C, 4 h for **1b–c**, **1f**, **1h**; (b) *tert*-butyl 4-[4-(4,4,5,5-tetramethyl-1,3,2-dioxaborolan-2-yl)phenyl]piperazine-1-carboxylate (**4**), XPhos Pd G2, K₃PO₄, butanol/H₂O, 100 °C, 4 h; (c) 4 M HCl in dioxane, MeOH, room temperature (rt), 30 min.

using recombinant ALK2 protein subsequently yielded a new series of inhibitors based on the 3,5-diphenylpyridine chemotype, typified by **K02288**,³⁶ **LDN-213844**, and **LDN-214117**.³⁷ More recently, the toolbox of compounds has been expanded through the discovery of a 3-(4-sulfamoylnaphthyl)pyrazolo[1,5-*a*]pyrimidine (modified **LDN-193189**) analog (**Compound 23**),³⁸ as well as inhibitors based on quinazolinone (**Compound 24**),³⁹ bis-heteroaryl pyrazole (**Compound 18p**),⁴⁰ and macrocyclic (**OD36**) scaffolds.⁴¹ At the time of writing, a number of ALK2 inhibitors such as **BLU-782** (**IPN60130**), **BCX9250**, and **KER-047** are being explored for FOP,⁴² and another, **Itacosertib** (**TP-0184** from Sumitomo-Tolero Pharma), has progressed into clinical trials (Phase I) as a treatment for DIPG.

Of the existing preclinical ALK2 inhibitors, **LDN-193189**, **LDN-212854**, and **LDN-214117** have been examined in orthotopic *in vivo* models of DIPG owing to their suitable brain penetration, pharmacokinetic (PK) properties, and general tolerability.^{27,43} While **LDN-212854** was found to be beneficial in a viral infection **ACVRI**^{R206H} mouse model,²⁷ both **LDN-193189** and **LDN-214117** showed significant 15 day prolongation of progression-free survival in mice bearing **ACVRI**^{R206H} patient-derived xenografts.⁴³ Given the positive *in vivo* outcome, we became interested in developing analogs of the lead compound **LDN-214117** into potential clinical candidates. To expedite efforts, we adopted an open science model centered on the newly created M4K (Medicines4Kids) Pharma Inc., itself owned by the Agora Trust Fund.^{44,45}

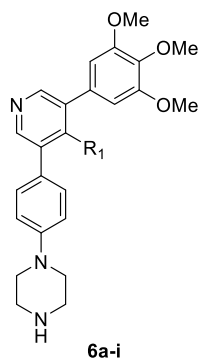
Although **LDN-214117** has been demonstrated to have reasonable kinome-wide selectivity and low toxicity,³⁷ we were particularly interested in increasing not only potency against ALK2 (to achieve a biochemical IC₅₀ < 20 nM and cellular IC₅₀ < 100 nM) but also the selectivity over the closely related type I TGFβ pathway receptor ALK5. Documented adverse effects of ALK5 inhibition include cardiotoxicity (valvular lesions), effects on bone growth (physeal dysplasia), and gastrointestinal inflammation,⁴⁶ so >50-fold selectivity for ALK2 over ALK5 in biochemical and cell-based assays was deemed essential to establish a desired safety profile and mitigate potential toxicity associated with long-term dosing. Parallel selectivity over ALK4

and ALK7 would be beneficial for similar reasons, particularly since ALK4 is also involved in myostatin signaling, the impairment of which can result in muscle atrophy.⁴⁷ Off-target toxicity related to other type I BMP pathway receptors may also be a concern given that inhibition of ALK1 has been associated with vascular effects (telangiectasia, edema, and congestive cardiac failure),⁴⁸ and ALK3 is implicated in the regulation of iron storage.⁴⁹ It should be noted, however, that ALK1-specific monoclonal antibody treatment administered to cancer patients did show a manageable safety profile with dosing up to 4.6 mg/kg being well tolerated.⁵⁰ A particular challenge in the development of selective, adenosine triphosphate (ATP)-competitive small-molecule kinase inhibitors is the high degree of structural homology evident in the conserved ATP binding domains. For example, the ALK3 kinase domain possesses 66% sequence identity with that of ALK5, illustrative of the high structural homology among type I receptors of both the BMP and TGFβ signaling pathways.³¹ Within the BMP or TGFβ families, even greater kinase domain sequence identity is evident between homologues such as ALK1–ALK2 (79%), ALK3–ALK6 (86%), and ALK4–ALK5 (90%).

Additional considerations for inhibitor design included adjusting the molecular weight, number of hydrogen bond donor (HBD) and hydrogen bond acceptor (HBA) atoms, number of rotatable bonds, cLogP, pK_a, topological polar surface area (tPSA), metabolic stability, and effective permeability to within the generally accepted parameters for successful CNS-directed drugs.^{51–53}

Using the well-characterized pyrazolo[1,5-*a*]pyrimidine inhibitor **LDN-193189** as a control, we conducted the primary assessment of compound potency and selectivity against ALK1, ALK2, ALK2 mutants (G328V, R206H, and R258G), ALK3, ALK4, ALK5, and ALK6 using the radiometric *in vitro* kinase assay performed by Reaction Biology Corporation. Cellular activity against ALK2 in HEK-293 cells was determined by means of a NanoBRET assay employing competitive displacement of a fluorescent tracer (PBI-6908) from the binding pocket by test compounds and generation of IC₅₀ values from the resultant reductions in bioluminescence resonance energy

Table 1. Inhibitory and Off-Target Activities of LDN-213844, LDN-214117, and 6a–i



Compound	R ₁	ALK2 ^a IC ₅₀ (nM)	ALK5 IC ₅₀ (nM)	Fold Selectivity	NanoBRET ALK2 ^a IC ₅₀ (nM)	DLA ALK5 IC ₅₀ (nM)	Cell-based Fold Selectivity
LDN-213844	[Redacted]	15 [*]	240 [*] 800 ^b	16 [*]	58 ^b	1350 ^b	23
		13 ^b		62			
		20 (G328V) 12 (R206H) 4 (R258G)					
LDN-214117	[Redacted]	24 [*]	3000 [*] >2000	125 [*]	239	>5000	>21
		115		>17			
		344 (G328V) 86 (R206H) 19 (R258G)					
6a	Me	13 ^c 8 (G328V) 9 (R206H) 13 (R258G)	2427 ^c	187	45 ^c 6 (G328V) 16 (G356D) 7 (Q207D) 12 (R206H)	2712 ^c	60
6b	Et	181	>5000	>28	589	>5000	>8
6c	cPr	42	4658	111	159	>5000	>31
6d	OMe	103	>5000	>49	233	>5000	>21
6e	NH ₂	461	>5000	>11	255	>5000	>20
6f	F	15	880	59	32	2183	68
6g	Cl	16	1330	83	57	9454	166
6h	CF ₃	67	>5000	>75	184	>5000	>27
6i	CN	3	731	244	15	679	45

^aLiterature values.³⁷ Measured values were determined using a radioactive biochemical kinase assay. ^bALK2 mutants are identified in parentheses. ^cAverage of duplicate measurements. ^dAverage of triplicate measurements.

transfer (BRET) ratios. A dual luciferase assay (DLA) was used to determine cellular activity against ALK5.

RESULTS AND DISCUSSION

Synthesis of C-4 Position Analogs. With reference to the cocrystal structure of the prototypic 3,5-diphenylpyridine inhibitor LDN-213844 bound to ALK2 (Figure 1B, PDB code 4BGG),³⁷ it was anticipated that substitutions at the C-4

position could potentially allow for stronger hydrogen bonding to the amide of H286 in the hinge region through exertion of an electronic effect at the nitrogen of the pyridyl ring. Furthermore, the inhibitor's bioactive conformation appears to involve a dihedral angle between the pyridyl and C-3 position 3,4,5-trimethoxyphenyl rings approaching 90°, a relatively high energy conformation (2.5 kcal/mol) that would be stabilized with the torsional restriction imposed by a sterically bulky C-4 position

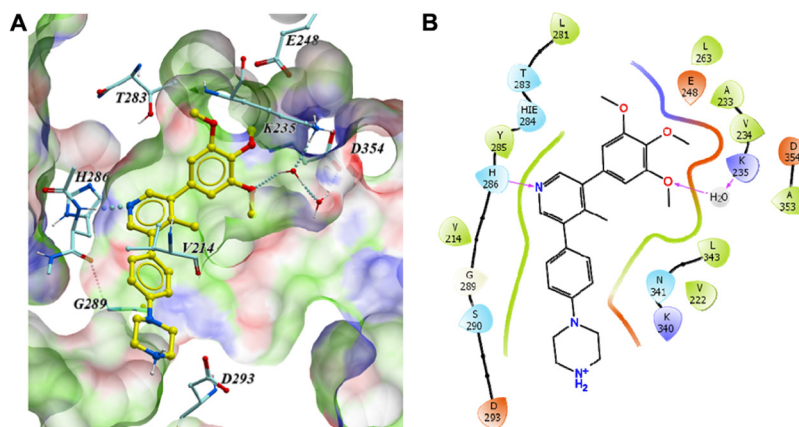


Figure 2. (A) Cocystal structure of **6a** (yellow) with ALK2 (PDB code 6SZM). Hydrogen bonds are established with H286 and K235. The 3,4,5-trimethoxyphenyl moiety of **6a** occupies a hydrophobic pocket (green) of ALK2 and is flanked by several hydrogen bond-donating (blue; K235) and hydrogen bond-accepting residues (red; D354 and E248). The protonated piperazine motif is in close proximity to D293, indicative of an electrostatic interaction. (B) Plot detailing the interactions of **6a** (black) within the ALK2 pocket.

substituent in a manner analogous to that of the C-2 position methyl substituent in LDN-214117. However, unlike in LDN-214117, this locking of the conformation would also impact the dihedral angle between the pyridyl ring and the C-5 position 4-piperazinophenyl ring, currently around 45°, pushing it toward 90° and potentially setting up a more favorable π - π stacking interaction of the phenyl ring between residues G289 and V214.

All C-4 position substituted analogs of LDN-213844 for our structure–activity relationship (SAR) study were synthesized using a route comprising an initial Suzuki–Miyaura coupling between commercially available 3,5-dihalopyridines (**1a–i**) and 3,4,5-trimethoxyphenylboronic acid (**2**) to yield intermediates **3a–i**, followed by a second coupling with 4-(4-*tert*-butoxycarbonylpiperazinyl)phenylboronic acid pinacol ester (**4**) and subsequent carbamate-protecting group removal from intermediates **5a–i** to yield the final inhibitors **6a–i** (Scheme 1). Although step *a* produced a significant amount of undesired decoupling product (~50%) when starting with symmetrical 3,5-dichloro- or 3,5-dibromopyridines (**1b–d** and **1f–h**), all steps were uniformly high yielding (>70%) and purification of intermediates **3a–i** was not required. A range of electron donating group (EDG) and electron withdrawing group (EWG) substitutions at the C-4 position (R_1) was readily accessible, and the corresponding inhibitors **6a–i** are summarized in Table 1 alongside reference compounds LDN-213844 and LDN-214117.

C-4 Position Analog SAR. Interestingly, the SAR of inhibitors **6a–i** revealed a generally higher potency against ALK2 for inhibitors bearing an EWG at the C-4 position (**6f–i**), with values near or below our set biochemical and cellular assay limits (20 and 100 nM, respectively). Compound **6h** was an outlier, perhaps due to negation of the trifluoromethyl group's strong EWG character by a presumptive, unfavorable steric effect. Compounds with a weak or strong EDG at the C-4 position (**6a–c** and **6d–e**, respectively) were generally less potent, although methyl substituted **6a** was a notable exception. Overall, this observed electronic effect was counter to what was anticipated, with the compounds bearing an EDG at the C-4 position expected to have a more basic pyridyl nitrogen capable of forming a stronger hydrogen bond interaction with the backbone amide of H286. Compounds **6a** and **6f–g** exhibited potencies similar to those reported for LDN-213844 and LDN-214117³⁷ although they were all considerably more potent than

the later inhibitor was in our hands (ALK2 IC_{50} = 115 nM). Inhibitor **6i** was particularly potent, and we believe it is the first reported IC_{50} < 5 nM inhibitor of ALK2.

Gratifyingly, all compounds showed an impressive level of selectivity for ALK2 over ALK5, equaling or exceeding levels exhibited by lead compounds LDN-213844 and LDN-214117. While generally high, this selectivity was relatively low in the biochemical assay for **6f** with R_1 = F. Given that this was the sterically smallest C-4 position substituent screened and resulted in ALK2 selectivity comparable to that of LDN-213844 where R_1 = H, increased steric bulk at the C-4 position may be at least a partial driver of selectivity through the enforcement of a favorable binding conformation. The same steric effect is likely seen in LDN-214117 where the C-2 position methyl group restricts rotation of the C-3 position trimethoxyphenyl moiety relative to the pyridyl core and produces an ALK2 selectivity that is both significantly greater than that of LDN-213844 and more in line with that of **6a** where R_1 = Me exerts a comparable steric influence.

Structural Basis for ALK2 Inhibition and Selectivity. Crystallographic efforts yielded a high-resolution (1.42 Å) cocystal structure of **6a** in the ATP pocket of the ALK2 Ser/Thr kinase domain (Figure 2A, PDB code 6SZM), confirming binding to the active A-loop DLG-in/ α C-helix-in conformation by means of a key ATP-mimetic hydrogen bond between the core pyridine nitrogen and the backbone amide of H286 in the hinge region. The C-3 position 3,4,5-trimethoxyphenyl moiety of **6a** occupies the hydrophobic pocket of ALK2 as expected, and the *meta*-methoxy group participates in a water-mediated hydrogen bond with K235. The aryl ring of the C-5 position 4-piperazinophenyl substituent stacks between G289 and V214, while the protonated secondary amine of the piperazine is in close proximity to D293 (5.11 Å between the 1-position piperazine nitrogen and D293 oxygen), suggestive of a solvent-mediated electrostatic ionic interaction.

As we were unable to obtain a cocystal structure of **6a** with ALK5, it is difficult to fully rationalize the compound's evident selectivity for ALK2. With reference to LDN-213844, it was suggested that selectivity may be a consequence of dynamic conformational differences between ALK2 and ALK5 in tandem with effects exerted by the small number of sequence changes in the ATP pocket (see the Supporting Information, Figure S1).³⁷ It can also be argued that the ATP pocket in many available

ALK5 cocystal structures shows a more open conformation than that of ALK2, the possible result of a smaller gatekeeper residue [S280 (ALK5 numbering) versus T283 (ALK2 numbering)]. Noticeable movement of the N-lobe away from the C-lobe in ALK5 structures changes the shape, volume, and dynamics of the ATP pocket, all of which have an effect on inhibitor binding. In addition, the conformational lock imposed on **6a** by the presence of the C-4 position methyl substituent enforces significant torsional angles ($\geq 45^\circ$) evident between the core pyridine and the C-3 and C-5 position substituents, potentially aiding a preferential fit within the ALK2 pocket.

C-4 Position Analog Off-Target Activity. Compounds **6a**, **6f–g**, and **6i** remained of interest given that they satisfied our ALK2 potency and selectivity criteria in both the biochemical and cell-based assays. Choosing **6a** as an exemplar from this smaller set, we first determined the compound's potency against available ALK2 mutants (G328V, R206H, and R258G) in the biochemical assay. As expected, potency was in line with that observed against wild-type (WT) ALK2, comparable to the values obtained for LDN-213844, and superior to those recorded for LDN-214117. Inhibitor **6a** also performed well when evaluated against ALK2 mutants (G328V, G356D, Q207D, and R206H) using the NanoBRET assay, showing that this favorable level of activity was undiminished in cells. It had previously been demonstrated that mutations in both the GS and Ser/Thr kinase domains of ALK2 had negligible effects on the kinase's affinity for ATP and type I kinase inhibitors,³⁷ so for reasons of protein availability and assay expense, we opted to screen the inhibitory activity of all other compounds in our studies exclusively against WT ALK2.

In addition to the primary focus of limiting activity against ALK5, we hoped for a degree of selectivity for ALK2 over other off-targets of concern such as ALK1, ALK3, and ALK4. Profiling of representative compound **6a** revealed it to be equipotent on ALK1 ($IC_{50} = 15$ nM) but with modest 33-fold selectivity over ALK3 ($IC_{50} = 428$ nM) and substantial 103-fold selectivity over ALK4 ($IC_{50} = 1336$ nM). This later selectivity over ALK4 is a notable improvement over the 36-fold selectivity exhibited by LDN-213844 ($IC_{50} = 462$ nM), again suggesting a possible role for the C-4 position methyl as a selectivity element. Compounds of interest **6f** (ALK4 $IC_{50} = 630$ nM), **6g** (ALK4 $IC_{50} = 962$ nM), and **6i** (ALK4 $IC_{50} = 257$ nM) also show improved 42-, 60-, and 86-fold selectivities (respectively) over ALK4, but all were less selective than **6a**. Although of less concern as an off-target, screening of **6a** against ALK6 revealed only slight selectivity on the order of 5-fold (ALK6 $IC_{50} = 68$ nM). All of these values are fully consistent with the aforementioned high degrees of structural homology among type I receptors of both the BMP and TGF β signaling pathways,³¹ but the selectivity windows relating to critical off-targets ALK3, ALK4, and ALK5 suggest the possibility of a meaningful safety profile. Although potent against ALK1, based on past work, it is anticipated that any ALK1-driven toxicity arising from an inhibitor similar to **6a** could be managed through an appropriate dosing level or regimen.⁵⁰ We did not have access to ALK7 during the course of this study and hence did not measure the potency of **6a** against that target.

As previously mentioned, LDN-214117 was demonstrated to have reasonable kinase-wide selectivity,³⁷ with improvement over pyrazolo[1,5-*a*]pyrimidine inhibitors such as LDN-193189.³⁰ At 1 μ M, LDN-214117 inhibited only 3.6% of kinases (~ 200) profiled by more than 50%, with ABL1, RIPK2, and TNIK being the most inhibited after ALK2.³⁷ We screened

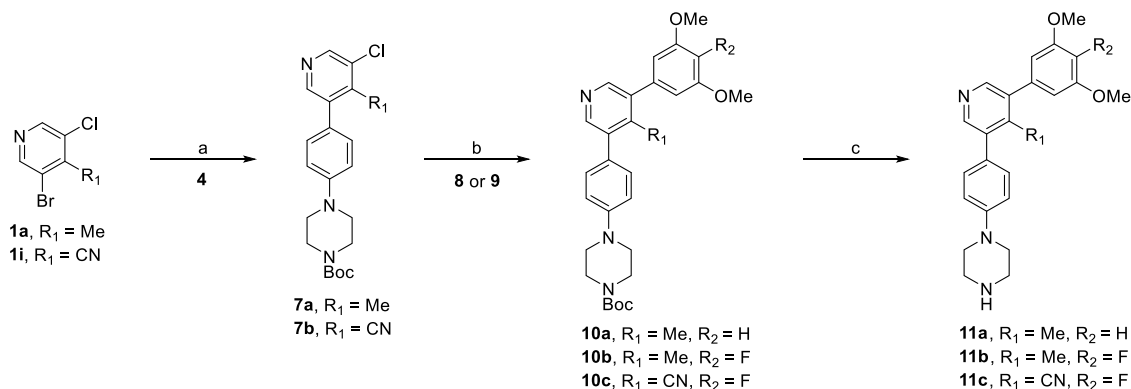
6a at 1 μ M against a significantly larger 374-member kinase set, finding remarkable selectivity with greater than 50% inhibition against only 2.1% of kinases (see the Supporting Information, Table S1). Of the eight kinases inhibited (ABL1, BRK, DDR1, MINK, NLK, SIK2, TNIK, and ZAK), **6a** was only significantly potent against DDR1 ($IC_{50} = 41$ nM) and TNIK ($IC_{50} = 96$ nM) (see the Supporting Information, Note S1), with IC_{50} values against the remaining six kinases in the 336–924 nM range.

To gauge the potential risk from another off-target related adverse drug reaction, **6a** was screened in the Eurofins Cerepanlabs *in vitro* SafetyScreen 44 panel (see the Supporting Information, Table S2). At 10 μ M, only five targets were inhibited more than 50%, with **6a** being the most potent against the cannabinoid CB₁ (97%) and adrenergic α_{2A} (90%) receptors, followed by activity against the sodium channel site 2 (72%), the human ether-a-go-go (hERG) potassium channel (69%), and the adrenergic α_{1A} (65%) receptor. A dose-response follow-up at 3 μ M on the highly inhibited targets showed a cannabinoid CB₁ receptor $IC_{50} = 1.72$ μ M and an adrenergic α_{2A} receptor $IC_{50} = 2.18$ μ M. With **6a** showing greater than 100-fold selectivity for ALK2 over these two targets, no significant concerns were registered in relation to these receptors.

Inhibition of the hERG potassium channel by **6a** warranted further investigation given that loss of function is associated with long-QT syndrome type-2 (LQT2) and increased risk of potentially fatal *torsades de pointes* cardiac arrhythmia *in vivo*.⁵⁴ Evaluation in the Charles River Laboratories ScreenPatch (patch clamp) assay found **6a** to be only a moderate inhibitor of the hERG potassium channel ($IC_{50} = 8.3$ μ M). To see if hERG potassium channel inhibition could be further attenuated through the incorporation of an EWG at the C-4 position, we also evaluated **6g** and **6i** but unfortunately found that both compounds were slightly more active with $IC_{50} = 2.7$ μ M and $IC_{50} = 6.0$ μ M, respectively. Although an hERG potassium channel $IC_{50} > 10$ μ M was desirable to limit the likelihood of cardiac toxicity, historic data pertaining to FDA-approved (tyrosine) kinase inhibitor drugs has shown that an $IC_{50} < 1$ μ M is regarded as problematic, while an $IC_{50} > 3$ μ M is generally acceptable.⁵⁵ As such, we considered these compounds to have a manageable hERG potassium channel inhibition profile, which could be further derisked in a preclinical setting through *in vivo* canine electrophysiology studies. In addition, we engaged in structural modifications to the C-3 position 3,4,5-trimethoxyphenyl moiety and the C-5 position 4-piperazinophenyl moiety, anticipating that those changes could potentially exert an influence on binding to the hERG potassium channel.

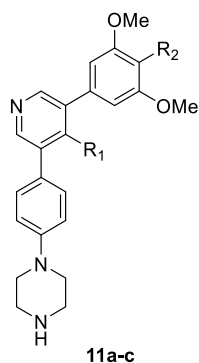
Screening of **6a** by colleagues at Charles River Laboratories against seven major cytochrome P450 (CYP) enzyme isoforms (1A2, 2B6, 2C8, 2C9, 2C19, 2D6, and 3A4M/3A4T) in human liver microsomes at 30 μ M showed the compound to be clean, with $IC_{50} > 30$ μ M on all targets except 3A4T ($IC_{50} > 9$ μ M). To evaluate the mutagenic potential of **6a**, a Mini-Ames assay was conducted at WuXi AppTec, concluding that the compound was negative for mutagenicity under the conditions of this study.

C-4 Position Substituent Selection. The activity and selectivity of inhibitors **6a**, **6f–g**, and **6i** provided us with four C-4 position substituents that appeared suitable for inclusion in further analogs. Given the inefficiency inherent in the synthesis of **6f–g** (Scheme 1, step a) and their highly similar biochemical and cellular activity profiles in relation to **6a**, we opted to move forward only with analogs of compounds **6a** and **6i**. The C-4 position methyl scaffold of **6a** was of particular interest given its

Scheme 2. Synthesis of Compounds 11a–c^a

^aReagents and conditions: (a) *tert*-butyl 4-[4-(4,4,5,5-tetramethyl-1,3,2-dioxaborolan-2-yl)phenyl]piperazine-1-carboxylate (**4**), Pd(dppf)Cl₂·DCM, Na₂CO₃, DMF/H₂O, 100 °C, 16 h; (b) 3,5-dimethoxyphenylboronic acid (**8**) or (4-fluoro-3,5-dimethoxyphenyl)boronic acid (**9**), XPhos Pd G2, K₃PO₄, butanol/H₂O, 100 °C, 4 h; (c) 4 M HCl in dioxane, MeOH, rt, 30 min.

Table 2. Inhibitory and Off-Target Activities of 6a and 11a–c



Compound	R ₁ / R ₂	cLogP LipE ^a	ALK2 IC ₅₀ (nM)	ALK5 IC ₅₀ (nM)	Fold Selectivity	NanoBRET ALK2 IC ₅₀ (nM)	DLA ALK5 IC ₅₀ (nM)	Cell-based Fold Selectivity
6a	Me / OMe	3.29 4.60	13 ^b	2427 ^b	187	45 ^b	2712 ^b	60
11a	Me / H	3.95 3.46	39	>5000	>128	440	>5000	>11
11b	Me / F	3.72 4.00	19	2206	116	98	7475	74
11c	CN / F	3.46 4.50	11	487	44	49	1511	31

^aLipE (lipophilic efficiency) = pIC₅₀ – cLog P, where pIC₅₀ = –log ALK2 IC₅₀ (nM). ^bAverage of triplicate measurements.

favorable kinome-wide selectivity and off-target profiles detailed above, although **6i**, despite its reduced cellular ALK2 selectivity, remained of interest because of its potency.

Synthesis of C-3 Position Analogs. Foundational SAR studies on **K02288**, **LDN-213844**, and **LDN-214117** done by our collaborators led to discovery of the C-3 position 3,4,5-trimethoxyphenyl substituent, an optimal group for providing interactions in the hydrophobic pocket as well as a water-mediated hydrogen bond to K235.^{36,37} Critical to this hydrogen bond formation is the methoxy group at the 3-position of the phenyl ring, with both the 3- and 4-position methoxy groups engaged in bidentate hydrogen bonding evident in select cocrystal structures. Deletion of the 4-position methoxy group

to produce a 3,5-dimethoxyphenyl moiety was tolerated, yielding almost equipotent compounds and suggesting that the phenyl ring was amendable to transformation.³⁷ Our own extensive efforts to modify the 3,4,5-trimethoxyphenyl moiety in the context of **LDN-213844** and **6a** analogs by eliminating or altering substituents were largely unproductive,⁵⁶ although limited success was achieved through replacement with a 2-fluoro-6-methoxybenzamide moiety to yield equipotent inhibitors with reduced off-target affinity for the hERG potassium channel (IC₅₀ > 30 μM).⁵⁷ While the benzamide effectively recapitulated the water-mediated hydrogen bond to K235, its increased polarity had the unfortunate ancillary effect of making

the compounds poorly brain-penetrant and limiting their usefulness for the treatment of DIPG.

The only suitable, novel modification to the 3,4,5-trimethoxyphenyl group that emerged from our SAR studies on the LDN-213844 scaffold was replacement of the 4-position methoxy with fluorine, putatively capable of participating in an analogous water-mediated hydrogen bond to K235. We then looked to incorporate the required 4-fluoro-3,5-dimethoxyphenyl group at the C-3 position of **6a** and **6i**, alongside the aforementioned 3,5-dimethoxyphenyl group. This was readily accomplished by modifying the iterative Suzuki–Miyaura coupling sequence previously used for preparing the C-4 position analogs, yielding compounds **11a–c** (Scheme 2). Common intermediates **7a–b**, prepared first by attaching the C-5 position *tert*-butyl-4-phenylpiperazine-1-carboxylate moiety, allowed for flexible, subsequent coupling of the C-3 position substituted phenyl group of choice (Table 2).

C-3 Position Analog SAR, Off-Target Activity, and Substituent Selection. While inhibitor **11a** exhibited considerably reduced activity against ALK2 in cells, inhibitors **11b–c** were found to have activity profiles very similar to those of **6a** and **6i**. Although potency against ALK2 was only slightly lower for **11b–c**, selectivity over ALK5 in the biochemical assay dropped in both cases, with the effect being more pronounced for **11c** (a drop from 244-fold to 44-fold) than for **11b** (a drop from 187-fold to 116-fold). Interestingly, even though cellular activity against ALK2 was more than halved for both compounds, selectivity over ALK5 remained comparable at 74-fold and 31-fold for **11b** and **11c**, respectively. The less than 50-fold selectivity over ALK5 evident for **11c** in both assays led us to prioritize **11b** as an analog of interest for which we also confirmed a slightly decreased 79-fold selectivity over ALK4 ($IC_{50} = 1503$ nM). We did not screen **11b** against ALK1, ALK2 mutants, ALK3, or ALK6 given the expectation of equipotency against these targets based on the patterns of activity evident from the screening of other compounds.

Screening of **11b** at 1 μ M against a 374-member kinase set, unsurprisingly, yielded greater than 50% inhibition against seven of the eight kinases inhibited by **6a** (ABL1, BRK, DDR1, MINK, SIK2, TNIK, and ZAK) although activity against NLK was diminished. In addition, **11b** registered marginal activity (51–61% inhibition) against six other kinases (HGK, KHS, LCK, LYN, MLCK2, and SIK3) for a profile that involved an overall inhibition rate of 3.5% (see the Supporting Information, Table S1).

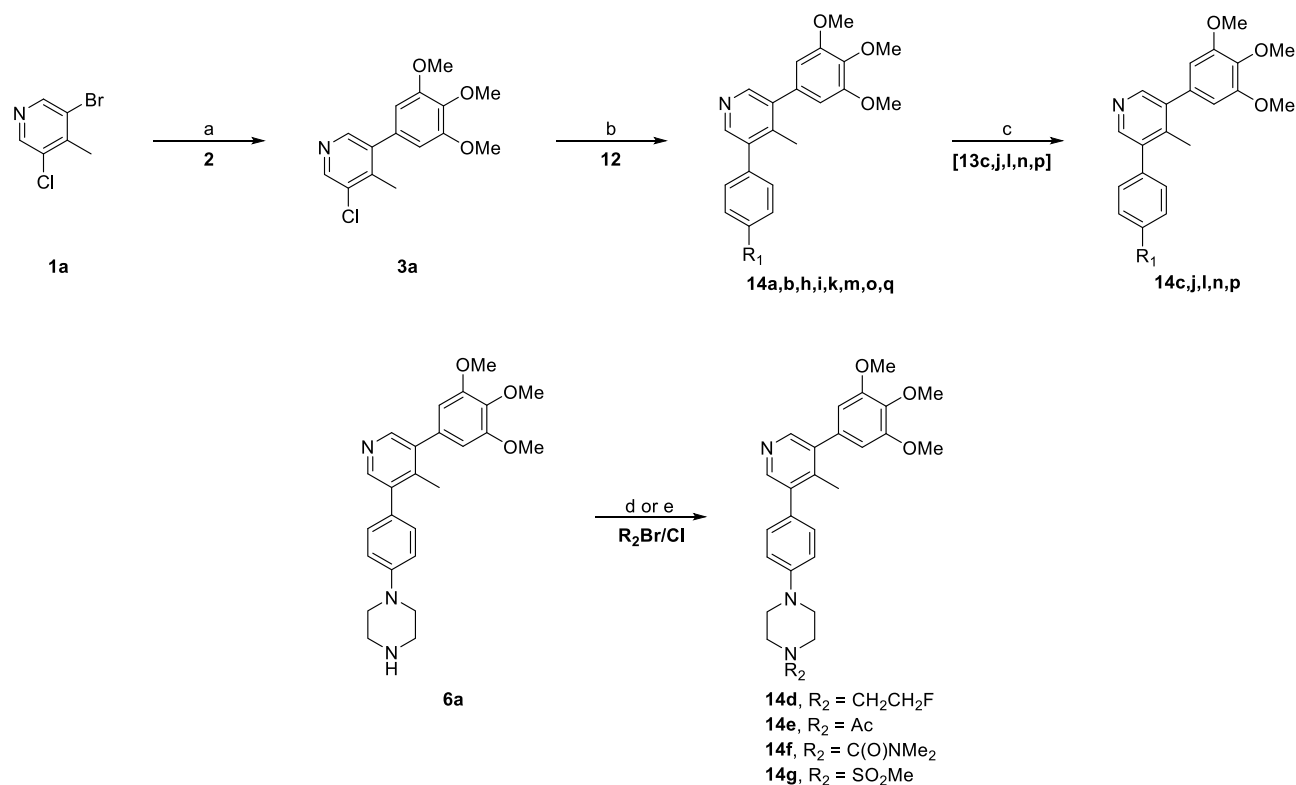
Activity against the hERG potassium channel as determined in the Charles River Laboratories ScreenPatch assay found **11b** to be a more potent inhibitor than **6a** with an $IC_{50} = 2.5$ μ M. While disappointing, this increased affinity for the hERG potassium channel was still within acceptable limits and viewed as a parameter that could potentially be impacted by replacement of the C-5 position 4-piperazinophenyl moiety in subsequent SAR studies. Compound **11b** was also marginally more active when screened in the seven-member CYP panel. While **6a** had an $IC_{50} > 30$ μ M against six of the isoforms, **11b** showed an $IC_{50} > 20$ μ M against only four targets with the 2C9 $IC_{50} = 7.3$ μ M, 2C19 $IC_{50} = 7.7$ μ M, and 3A4T $IC_{50} = 14.3$ μ M.

While **11b** was, in aggregate, a slightly inferior inhibitor with respect to **6a** by the parameters detailed above, it constituted the only viable C-3 position analog that warranted further development. Aside from its comparable biochemical and cell-based activity on ALK2, **11b** is a less polar compound ($cLog P = 3.72$ and $tPSA = 46$ \AA^2) than **6a** ($cLog P = 3.29$ and $tPSA = 55$

\AA^2),⁵⁸ suggesting it could potentially achieve a greater degree of brain penetration. As with the possibility to modify affinity toward the hERG potassium channel, changes in the C-5 position 4-piperazinophenyl moiety of **6a** were also viewed as a way to achieve $tPSA$ values similar to that of **11b** while preserving the C-3 position 3,4,5-trimethoxyphenyl moiety.

Synthesis of C-5 Position Analogs. With the C-3 and C-4 position substituents set, we endeavored to make changes to the C-5 position 4-piperazinophenyl moiety in an attempt to maintain or increase the activity against ALK2 shown by **6a** and decrease the activity against the hERG potassium channel while remaining cognizant of several physiochemical parameters. In order for small-molecule inhibitors to penetrate the BBB and exert a pharmacological effect, their lipophilicity ($cLog P$), basicity (pK_a), $tPSA$, and number of HBD/HBA (among other factors) ideally fall within a range of recommended values.^{51–53} Although enhanced drug potency and permeability are often a function of increased lipophilicity, a $cLog P < 5$ is considered optimal to avoid potential concomitant increases in nonspecific tissue binding, which would ultimately decrease the concentration of free drug at its intended site of action within the brain. Possession of a positive charge at physiological pH 7–8 favors brain permeation, so amine-containing compounds with a $pK_a = 7.5–10.5$ are ideal despite the potential for issues with hERG potassium channel binding. Keeping the $tPSA < 60–70$ \AA^2 , the number of HBD < 3 (CNS drugs have a mean of 1.1), and the number of HBA < 7 are also favorable for BBB penetration and limiting recognition by efflux transporters such as P-glycoprotein (P-gp).^{52,53} The calculated values for these primary metrics⁵⁸ informed our selection of suitable C-5 position substituents, the focus being on groups that would recapitulate, improve on, or not grossly deviate from the parameters of **6a** with a $cLog P = 3.29$, $pK_a = 8.60$, $tPSA = 55$ \AA^2 , HBD = 1, and HBA = 6.

The binding mode evident in the ALK2-**6a** cocrystal structure (Figure 2) has the phenyl ring of the C-5 position 4-piperazinophenyl substituent stacking between G289 and V214, so we opted to retain the unmodified phenyl ring in future analogs while focusing on changes to the piperazine consistent with the physiochemical parameters detailed above. Again, published SAR studies pertaining to the C-5 position³⁷ as well as our own wide-ranging exploratory efforts⁵⁶ built confidence in further narrowing the scope of our modifications. The challenge, however, was to attenuate the activity on the hERG potassium channel under these constraints, given that the C-5 position 4-piperazinophenyl substituent constitutes an ideal pharmacophore against the channel based on known ligand-based pharmacophore and QSAR models.^{59,60} While it is known that increasing the polarity of the drug molecule (lowering the $cLog P$) effectively reduces activity against the hERG potassium channel, our efforts to employ this strategy met with limited success as they produced a concomitant decrease in BBB penetration.⁵⁷ Consequently, we focused our efforts on discrete structural modifications to the putative hERG potassium channel binding motif, which would affect the sterics and/or conformation around the 1-position piperazine nitrogen or reduce its basicity (lower the pK_a). These later strategies are known to effectively disrupt the cation π -stacking interactions between the basic amine-containing hERG potassium channel blockers and aromatic residues within the cavity of the channel at physiological pH and could be executed within the optimal parameters for CNS drugs described above.

Scheme 3. Synthesis of Compounds 14a–q^a

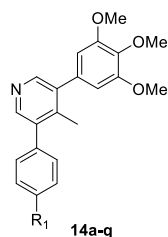
^aReagents and conditions: (a) 3,4,5-trimethoxyphenylboronic acid (**2**), Pd(dppf)Cl₂·DCM, Na₂CO₃, DMF/H₂O, 100 °C, 16 h; (b) 4-(R₁)phenylboronic acid or pinacol ester (**12a–c** and **12h–q**), XPhos Pd G2, K₃PO₄, butanol/H₂O, 100 °C, 4 h; (c) [**13c**, **13j**, **13l**, **13n**, **13p**], 4 M HCl in dioxane, MeOH, rt, 30 min; (d) R₂OTs, triethylamine (TEA), acetonitrile, 100 °C, 16 h for **14d**; (e) R₂Cl, *N,N*-diisopropylethylamine (DIPEA), tetrahydrofuran (THF), rt, 1 h.

Analogs were accessed efficiently via common intermediates **3a** and **6a** incorporating the C-3 position 3,4,5-trimethoxyphenyl group, with the idea that analogs incorporating the alternate 4-fluoro-3,5-dimethoxyphenyl group could subsequently be prepared using only the optimal C-5 position substituents. Once again, the same sequential Suzuki–Miyaura coupling approach used for all previous analogs was employed to prepare new C-5 position analogs **14a–c** and **14h–q**, with analogs **14d–g** accessed directly from **6a** through straightforward alkylation, acetylation, carbamoylation, or sulfonylation, respectively (Scheme 3). Synthesis was facilitated by the commercial availability of the requisite 4-substituted phenylboronic acids or pinacol esters (**12a–c** and **12h–q**), and the generally high coupling yields (>70%) were encouraging for potential future scale-up requirements. An additional carbamate-protecting group removal step was required for the conversion of intermediates **13c**, **13j**, **13l**, **13n**, and **13p** to final inhibitors **14c**, **14j**, **14l**, **14n**, and **14p**, but additional purification of the final product was not required if previously conducted on the respective intermediate (Table 3).

C-5 Position Analog SAR, Off-Target Activity, and Substituent Selection. While unsurprising that methylation of **6a** resulted in a compound with an almost identical activity and selectivity profile (**14a**), we were disappointed to find that sterically shielding the 1-position piperazine nitrogen with a larger isopropyl group (**14b**) adversely impacted both the cellular activity on ALK2 and selectivity over ALK5. When the steric bulk was made adjacent to the same nitrogen through methylation of the C-2 and C-6 piperazine ring positions (**14c**),

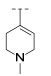
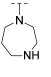
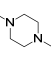
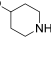
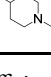
cellular activity against ALK2 was preserved, but selectivity over ALK5 still remained below our set 50-fold lower limit. While not entirely satisfactory, **14b–c** did still show reasonable levels of activity against ALK2 while maintaining cLog *P*, p*K_s*, and tPSA values close to those of **6a**, so we used them to evaluate whether steric shielding of the 1-position piperazine nitrogen held any potential for mitigating activity on the hERG potassium channel. Unfortunately, both compounds were slightly more potent with hERG IC₅₀ = 3.1 μM for **14b** and hERG IC₅₀ = 5.9 μM for **14c**.

Reluctant to further increase the overall molecular weight by exploring bulkier alkylic substituents, we turned our attention to attenuating the basicity of the 1-position piperazine nitrogen. It is known that introduction of fluorine as a hydrogen atom replacement in alkyl substituted amines can effectively modulate their basicity, with significant p*K_a* shifts observed when the fluorine is installed at either the β-position (Δp*K_a* −1.7) or the γ-position (Δp*K_a* −0.7).⁶¹ To that end, we prepared compound **14d** bearing a 2-fluoroethyl group whose calculated p*K_a* = 7.49 was a full 1.11 units lower than that of **6a**. While comparably active against ALK2 in the biochemical assay, cellular activity (IC₅₀ = 178 nM) was greatly diminished, placing the compound well beyond our acceptable limit. Acetylation, carbamoylation, and sulfonylation of the nitrogen designed to effectively abolish basicity while introducing oxygen atoms with HBA potential afforded compounds **14e–g**. Inhibitors **14e–f** were poorly active against ALK2 in cells, while **14g** exhibited activity similar to that of **6a** with the benefit of a near doubling in selectivity over ALK5 to 108-fold. Significantly, **14g** had an hERG IC₅₀ > 50 μM, likely resulting from both the decrease in basicity and a 26 Å²

Table 3. Inhibitory and Off-Target Activities of 6a and 14a–q^b

Compound	R ₁	cLogP pK _a tPSA (Å ²) LipE ^a	ALK2 IC ₅₀ (nM)	ALK5 IC ₅₀ (nM)	Fold Selectivity	NanoBRET ALK2 IC ₅₀ (nM)	DLA ALK5 IC ₅₀ (nM)	Cell-based Fold Selectivity	hERG IC ₅₀ (μM)
6a		3.29 8.60 55 4.60	13 ^b	2427 ^b	187	45 ^b	2712 ^b	60	8.3
14a		3.74 8.56 47 4.31	9	4847	539	56	>5000	>89	-
14b		4.58 8.65 47 3.57	7	2236	319	73	1824	25	3.1
14c		4.32 8.74 55 3.78	8	1050	131	40	1427	36	5.9
14d		3.99 7.49 47 3.78	17	3215	189	178	>5000	>28	-
14e		2.88 - 64 4.78	22	2524	115	267	>5000	>19	-
14f		3.97 - 67 4.43	4	>5000	>1250	149	>5000	>34	-
14g		3.30 - 81 4.24	29	1983	68	59	6392	108	>50
14h		3.30 - 53 4.25	28	2356	84	334	>5000	>15	-
14i		2.33 - 77 5.47	16	1229	77	169	>5000	>30	-
14j		3.93 9.84 52 4.12	9	1745	194	54	3421	63	-
14k		4.21 9.79 43 3.94	7	>5000	>714	29	3326	115	4.8
14l		3.83 9.17 52 4.47	5	>5000	>1000	47	7532	160	3.4

Table 3. continued

Compound	R ₁	cLogP pK _a tPSA (Å ²) LipE ^a	ALK2 IC ₅₀ (nM)	ALK5 IC ₅₀ (nM)	Fold Selectivity	NanoBRET ALK2 IC ₅₀ (nM)	DLA ALK5 IC ₅₀ (nM)	Cell-based Fold Selectivity	hERG IC ₅₀ (μM)
14m		4.11	14	2520	180	102	7803	77	-
		9.12							
		43							
		3.74							
14n		3.33	13	3050	235	83	4531	55	-
		9.26							
		55							
		4.56							
14o		3.92	20	2643	132	108	>5000	>46	-
		3.48							
		47							
		3.78							
14p		3.36	6	2854	476	31	1908	62	8.1
		9.45							
		61							
		4.86							
14q		3.64	6	1650	275	67	2094	31	-
		9.40							
		53							
		4.58							

^aLipE (lipophilic efficiency) = pIC₅₀ - cLog P, where pIC₅₀ = -log ALK2 IC₅₀ (nM). ^bAverage of triplicate measurements.

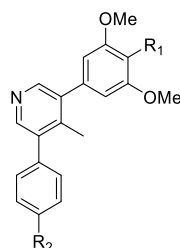
increase in tPSA over **6a** to 81 Å². Although this value was beyond the generally favorable tPSA < 60–70 Å² range for CNS drugs, we felt that further evaluation of this compound was warranted.

Having demonstrated with compound **14g** that it was possible to achieve potency against ALK2 in the absence of a basic piperazine nitrogen, we endeavored to replace the piperazine with morpholine (**14h**) and thiomorpholine 1,1-dioxide (**14i**). Designed to remove the 1-position piperazine nitrogen entirely and access the potential HBA capacity offered by oxygen, these compounds showed poor cellular activity against ALK2 despite having reasonable values in the biochemical assay. Removal of the other, less basic 4-position piperazine nitrogen was also examined *via* the synthesis of piperidine-containing inhibitors **14j–k** and 1,2,3,6-tetrahydropyridine-containing inhibitors **14l–m**, both with different ring topology and conformation in an attempt to influence hERG potassium channel binding. Inhibitor **14j** was found to have an activity and selectivity profile almost identical to that of **6a**, but we were particularly attracted by its methylated analog **14k**, which exhibited superior cellular activity (ALK2 IC₅₀ = 29 nM) and selectivity over ALK5 (115-fold). Interestingly, in the 1,2,3,6-tetrahydropyridine containing inhibitor pair, unmethylated analog **14l** was superior to **14m** in both activity (ALK2 IC₅₀ = 47 nM) and selectivity over ALK5 (160-fold). Unfortunately, neither the changed electronics nor the conformation embodied in the piperidine and 1,2,3,6-tetrahydropyridine rings of **14k–l** served to decrease activity against the hERG potassium channel, with the compounds registering an hERG IC₅₀ = 4.8 μM and hERG IC₅₀ = 3.4 μM, respectively. However, in contrast to **6a** (cLog P = 3.29, tPSA = 55), **14k** was of particular interest given its increased lipophilicity (cLog P = 4.21, tPSA = 43) and attendant potential for greater BBB penetration. We replaced the C-3 position 3,4,5-trimethoxyphenyl group of **14k** with the previously explored 4-fluoro-3,5-dimethoxyphenyl group to access an even more lipophilic analog (cLog P = 4.65, tPSA = 35) but did not pursue the resulting compound further as it showed decreased cell-

based activity (ALK2 IC₅₀ = 77 nM) and poorer selectivity over ALK (61-fold).⁵⁶

Further attempts at instituting conformational changes around the piperazine ring involved its enlargement to homopiperazine (**14n**) and introduction of a benzylic carbon linker between it and the C-5 position phenyl ring (**14o**). Both changes produced slightly less active and selective compounds in cells, but the activity of **14o** raised the possibility of employing an analogous spacer in combination with the piperidine moiety found to be potent in compounds **14j–k**. To overcome the potential metabolic liabilities associated with benzylic carbons, we switched to a phenolic oxygen linker for the synthesis of **14p–q**. We were pleasantly surprised to see that **14p** in particular had an activity and selectivity profile comparable to that of **6a** and that this profile extended its activity against the hERG potassium channel (IC₅₀ = 8.1 μM). While there was no reduction in the hERG potassium channel binding affinity, **14p** did still offer a viable alternative chemotype for advancement into further studies.

While we deemed it unnecessary to screen **14g**, **14k–l**, and **14p** against ALK1, ALK2 mutants, ALK3, or ALK6 based on the known pattern of activity for this class of compounds (see above), we did spot-check the activity of these compounds against ALK4. **14k–l** had an ALK4 IC₅₀ > 2000 nM, with only relatively marginal activity shown by **14g** (ALK4 IC₅₀ = 1131 nM) and **14p** (ALK4 IC₅₀ = 1363 nM) corresponding to 39-fold and 227-fold selectivity for ALK2, respectively. Although the reduced selectivity of **14g** over ALK4 was of some concern, we still felt that analysis of its absorption, distribution, metabolism, and excretion (ADME) and PK properties was warranted based on the compound's relatively high cellular potency against ALK2, significant selectivity over ALK5, and lack of affinity for the hERG potassium channel. As an interesting, representative piperidine-containing inhibitor, we screened **14k** at 1 μM against the 374-member kinase panel, finding >50% inhibition against only 1.9% of the kinases (see the Supporting Information, Table S1). All of the seven kinases inhibited

Table 4. *In Vitro* ADME Parameters for 6a, 11b, 14g, 14k–l, and 14p^e

6a, 11b, 14g, 14k–l, 14p

Compound	R ₁	R ₂	Microsomal Stability Assay ^a		Caco-2 Permeability Assay ^{b,c}			PPB Assay	
			MLM (%)	HLM (%)	$P_{\text{app AB}}$ (10 ⁻⁶ cm/s)	$P_{\text{app BA}}$ (10 ⁻⁶ cm/s)	Efflux Ratio	Binding (%)	Free (%)
6a	OMe		64.6 ^d	71.4 ^d	5.4 ^d	8.0 ^d	1.5	94.3 ^d	5.7 ^d
11b	F		65.8 ^d	83.7 ^d	1.8 ^e	4.9	2.7	99.6	0.4
14g	OMe		100	83.6	34.5	33.8	1.0	-	-
14k	OMe		55.5	71.2	9.7	8.1	0.8	95.0	5.0
14l	OMe		73.9	68.0	2.9	3.9	1.3	-	-
14p	OMe		39.3	62.1	4.1	9.4	2.3	-	-

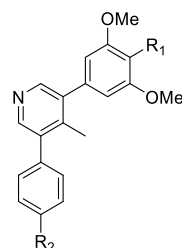
^aStability classification: stable (>70%), moderately stable (20–70%), or unstable (<20%) compound remaining. ^bPermeability classification: low ($P_{\text{app}} < 1$), medium ($P_{\text{app}} 1-3$), or high ($P_{\text{app}} > 3$) $\times 10^{-6}$ cm/s. ^cEfflux ratio (BA/AB) classification: negative (ratio < 2), minor/moderate (ratio 2–7), or high (ratio > 7). ^dAverage of duplicate measurements. ^ePoor post-assay recovery in A to B chambers possibly due to low aqueous solubility, high lipophilicity, nonspecific binding to plastics or cells, and/or poor intracellular stability of the test article.

(ABL1, BRK, DDR1, LYN, MINK, TNIK, and ZAK) had also been inhibited by 6a and/or 11b.

***In Vitro* ADME.** Presented with six compounds exhibiting the structural attributes of a potentially successful CNS drug while meeting our criteria for activity against ALK2, selectivity over ALKS, and binding to the hERG potassium channel, we moved to evaluate the *in vitro* stability, permeability, and plasma protein binding (PPB) of 6a, 11b, 14g, 14k–l, and 14p (Table 4). Phase I (CYP enzymes only) metabolic stability of the compounds was examined at 1 μ M in both mouse and human liver microsomes (MLM and HLM) following a 60 min incubation period at 37 °C, permeability was assessed using a Caco-2 assay, and

heparinized pooled human plasma coupled with a compound concentration of 5 μ M and 4 h incubation period at 37 °C was used for PPB determination.

We were pleased to find that across both the MLM and HLM assays, all of the compounds could be classified as being at least moderately stable (20–70% remaining), with some showing higher degrees of stability (>70% remaining). Compound 14p appeared to be the most labile, although it still demonstrated adequate stability to remain of interest. While it had been reported that the piperazine moiety of LDN-193189 is a metabolic liability,³⁸ the motif did not appear to present any significant issue in the context of our 3,5-diphenylpyridine class

Table 5. *In Vivo* PK and ADME Parameters for 6a, 11b, 14g, 14k–l, and 14p^c

6a, 11b, 14g, 14k–l, 14p

Compound	R ₁	R ₂	PK in Female SCID Mice and Male SD Rats ^a (n = 3)						
			2 mg/kg IV		10 mg/kg PO				
			Cl (mL/min/kg)	V _{ss} (L/kg)	t _{1/2} (h)	C _{max} (μM)	AUC _{inf} (h·μM)	F (%)	C _{brain} /C _{plasma} @ 4 h
6a	OMe		12.7 <i>22.1</i>	2.05 <i>5.22</i>	3.11 <i>3.58</i>	6.16 <i>1.28</i>	51.7 <i>17.4</i>	100 <i>96</i>	0.90 ^b
11b	F		17.1 <i>22.6</i>	2.77 <i>6.62</i>	3.68 <i>7.59</i>	3.19 <i>0.81</i>	22.7 <i>13.4</i>	95 <i>74</i>	1.41 <i>2.03^c</i>
14g	OMe		7.90	0.48	0.80	1.43	2.97	7	-
14k	OMe		8.90 <i>15.1</i>	2.44 <i>4.33</i>	3.67 <i>3.90</i>	4.74 <i>1.16</i>	32.4 <i>12.9</i>	74 <i>50</i>	0.82 <i>1.55^c</i>
14l	OMe		3.84	1.66	6.02	6.62	82.5	79	0.43
14p	OMe		6.00	2.23	7.70	4.71	65.8	96	-

^aItalicized table entries. ^bMale CD-1 mice at 2 h. ^cCompound administered at 100 mg/kg PO.

inhibitors with a half-life greater than 60 min apparent for all compounds.

Caco-2 permeability values were also high, with $P_{app_AB} \geq 3 \times 10^{-6}$ cm/s for all compounds except for 11b. Although the compound was found to be moderately permeable with a $P_{app_AB} = 1.8 \times 10^{-6}$ cm/s, poor post-assay recovery (<15%) for this compound, possibly a function of its increased lipophilicity, rendered the value less accurate. It also appeared that compounds 6a, 14g, and 14k–l were not subject to P-gp-mediated efflux, with 11b and 14p being only moderately so. These low efflux ratios, coupled with high P_{app_AB} values and microsomal stability, suggested that all compounds were suitable candidates for *in vivo* analysis.

Measurement of PPB for 6a (cLog $P = 3.29$), 11b (cLog $P = 3.72$), and 14k (cLog $P = 4.21$) showed 6a and 14k to have comparable, “druglike” free fractions (5.7 and 5.0%, respectively) despite their difference in lipophilicity. Although the 0.4% free fraction of 11b appears suboptimal in comparison, current understanding reveals that *in vitro* PPB does not determine the actual unbound concentration in plasma *in vivo*, and as such, optimizing for PPB in drug design is not recommended.⁶² For drugs targeting the CNS, it is suggested that efforts should focus on reducing drug efflux transport at the BBB to achieve a high unbound brain concentration and to use PPB and brain tissue binding to calculate the unbound brain to

unbound plasma concentration ratio for brain distribution assessment.

In Vivo PK and ADME. Given the favorable *in vivo* PK properties, suitable brain penetration, and general tolerability of LDN-214117 facilitating its successful use in orthotopic *in vivo* models of DIPG,⁴³ we felt confident that our modified, yet structurally related compounds would exhibit comparable or superior characteristics. To that end, we initially chose to evaluate the *in vivo* PK profiles of **6a**, **11b**, **14g**, **14k–l**, and **14p** in female CB17 SCID mice following 2 mg/kg IV ($n = 3$) and 10 mg/kg PO ($n = 3$) dosing in a formulation of 5% dimethyl sulfoxide (DMSO), 47.5% poly(ethylene glycol) (PEG) 400, and 47.5% deionized water with 10% Tween80. The inhibitors were all well tolerated, with no adverse effects observed in any test group allowing for successful readout of all parameters (Table 5).

Assessment in the IV arm showed clearance (Cl) for all compounds well below our set 30 mL/(min kg) upper limit, with **11b** showing the highest rate at 17.1 mL/(min kg). The steady-state volume of distribution (V_{ss}) was uniformly favorable ($V_{ss} = 1–3$ L/kg), with the exception of **14g** ($V_{ss} = 0.48$ L/kg). With **14g** also registering a half-life ($t_{1/2}$) under an hour ($t_{1/2} = 0.80$ h), a peak serum concentration (C_{max}) barely above our set 1 μ M lower limit ($C_{max} = 1.43$ μ M), total exposure (area under curve, AUC_{inf}) an order of magnitude lower than that of the other compounds ($AUC_{inf} = 2.97$ h· μ M), and bioavailability (F) that was grossly suboptimal ($F = 7\%$), the compound was a distinct outlier. Despite its considerable stability in the MLM/HLM assays and high degree of permeability in the Caco-2 assay, **14g** performed so poorly *in vivo* that we opted to drop the compound from further consideration.

To evaluate the viability of an alternate, DMSO-free vehicle for dosing and its effect on exposure, we opted to convert **6a** to both its hydrochloride (HCl) and mesylate (MsOH) salt forms by taking advantage of the 1-position piperazine nitrogen's basicity. Subsequent administration of **6a-HCl** and **6a-MsOH** in a formulation of 0.5% aqueous methylcellulose at 25 mg/kg PO to NOD SCID mice showed that both increased exposure levels relative to the free base control **6a** at the 0.5, 1, 2, and 6 h time points studied. Although similar in their effect, **6a-HCl** proved marginally superior and, at the reference time point of 1 h, resulted in a 22% increase in plasma concentration *versus* **6a** ($C_{plasma} = 9.11$ μ M for **6a-HCl**, while $C_{plasma} = 7.46$ μ M for **6a**). Subsequent preparation and screening of **11b-HCl** in the 0.5% aqueous methylcellulose vehicle produced a comparable improvement in exposure *versus* the free base **11b**.

Compounds **6a**, **11b**, and **14p** were found to be significantly more bioavailable than LDN-214117 ($F = 75\%$),⁴³ with **14k–l** showing more comparable values. The $t_{1/2}$ of all compounds (other than **14g**) matched or exceeded that of LDN-214117 ($t_{1/2} = 3.91$ h), but evaluation of relative C_{max} and AUC_{inf} values is more difficult given the differential dosing across the two trials (5 mg/kg PO in BALB/c mice for LDN-214117).⁴³ With PK parameters aligned or superior to those of LDN-214117, it was imperative to determine how well these compounds could potentially function in the CNS.

Determination of BBB penetration was conducted for **6a**, **11b**, and **14k–l**, opting to remove **14p** from the analysis given its broadly similar PK profile and extra HBA (the phenolic oxygen) we felt could be a liability. At a dose of 10 mg/kg PO in female CB17 SCID mice ($n = 3$), **6a**, **11b**, and **14k** showed exceptional brain-to-plasma ratios (C_{brain}/C_{plasma} or B/P) of 0.90, 1.41, and

0.82, respectively (Table 5). Although not measured under comparable conditions and at the same time point, a B/P of 0.80 ($C_{brain} = 10.94$ μ M) was reported for LDN-214117 at 2 h after 25 mg/kg PO dosing,⁴³ making **11b** a considerably more CNS-penetrant compound. Even **6a** appears to have a modest advantage in BBB penetration, with **14k** more akin to LDN-214117. A dose-dependency was observed for the B/P ratios of the two more lipophilic compounds, with increased values observed for both **11b** ($B/P = 2.03$ with a $C_{brain} = 33$ μ M) and **14k** ($B/P = 1.55$ with a $C_{brain} = 39$ μ M) following 100 mg/kg PO dosing in the same mouse strain ($n = 3$). While these values are exceptional, the efficiency of drug delivery across the BBB is better described by looking at the ratio of the unbound brain concentration ($C_{u,brain}$) to the unbound plasma concentration ($C_{u,plasma}$) at steady state, $K_{p,uu}$.⁶² Measuring these concentrations at the 2 h time point following 1 mg/kg IV dosing of **6a** in male CD-1 mice ($n = 3$), we found $C_{u,brain} = 3.7$ nM (3% of $C_{brain} = 123$ nM because $m-BTB = 97\%$) and $C_{u,plasma} = 14$ nM (9% of $C_{plasma} = 156$ nM because $m-PPB = 91\%$), so $K_{p,uu} = 0.3$. Although a $K_{p,uu} < 1$ is indicative of active efflux at the BBB, $K_{p,uu} = 0.3$ is in-line with a significant number of approved CNS drugs⁶² and, as such, was quite acceptable.

With compound **14l** showing relatively low BBB penetration ($B/P = 0.43$), we opted to evaluate the PK of only **6a**, **11b**, and **14k** in a second rodent species, dosing male SD rats at 2 mg/kg IV ($n = 3$) and 10 mg/kg PO ($n = 3$). Notably, $t_{1/2}$ values were comparable to or improved (as with **11b**) *versus* those observed in mice, although C_{max} , AUC_{inf} , and F metrics were uniformly diminished (Table 5, italicized entries). Compound **6a** emerged as the best performer, retaining both a decent maximum concentration ($C_{max} = 1.28$ μ M) and bioavailability ($F = 96\%$).

The evident oral bioavailability across two rodent species prompted us to conduct dose escalation trials with **6a**, **11b**, and **14k** to establish the linearity of C_{max} and AUC_{inf} and administration of the compounds at 10, 25, 50, and 100 mg/kg PO in female CB17 SCID mice ($n = 3$ per treatment) showed a high degree of dose-dependent correlation ($r^2 > 0.95$) across both parameters. The absence of any observable behavioral or physical abnormalities in the mice after 24 h at the highest dose of 100 mg/kg PO suggested we could test that limit in a prolonged maximum tolerated dose (MTD) study. As we were anticipating the use of **6a** for an *in vivo* C57BL/6 mouse FOP model to demonstrate ALK2^{R206H} target engagement, we opted to conduct the MTD study in that strain. Oral dosing over 5 days at 25 mg/kg once a day (QD) and twice a day (BID), 50 mg/kg QD, and 100 mg/kg QD showed **6a** to be well tolerated with no deaths, body weight loss (<5%), or gross pathology observed. Plasma concentrations increased linearly with dose ($r^2 > 0.95$), and significant brain exposure was also observed. As with **11b** and **14k**, an increase in B/P ratios was recorded at the 4 h time point following the increased doses, with $B/P = 1.5$, 1.8, and 1.1 for **6a** at 25, 50, and 100 mg/kg QD, respectively.

In Vitro Biology and In Vivo Mouse Models. Screening of the lead inhibitors **6a**, **11b**, and **14k** in a panel of patient-derived ACVR1 mutant and WT cell lines showed particularly significant growth inhibition of SU-DIPG-XXI (ACVR1^{G328W}) and HSJD-DIPG-007 (ACVR1^{R206H}) cells, with a $GI_{50} < 250$ nM across both lines for all compounds (except **14k** against HSJD-DIPG-007 with a $GI_{50} = 2.1$ μ M)⁵⁶ coupled to an observed decrease in *ID1* expression (>50%). These *in vitro* results, the aggregate properties of **6a**, **11b**, and **14k**, and their scalable syntheses (50 g quantities of each were prepared by GL Chemtec International Ltd. through an in-kind contribution) led us to select these

Table 6. Alignment of M4K2009, M4K2117, and M4K2163 with the Target Product Profile

	Target Product Profile	M4K2009 (6a)	M4K2117 (14k)	M4K2163 (11b)
Physicochemical Properties⁵⁷				
Molecular Weight	<450	419.53	432.56	407.49
H-bond Donors (HBD)	<3 (pref. 1)	1	0	1
H-bond Acceptors (HBA)	<7	6	5	5
Rotatable Bonds	<8	6	6	5
cLogP	<5	3.29	4.21	3.72
pK _a	7.5-10.5	8.60	9.79	8.60
tPSA (Å ²)	<60-70	55	43	46
Potency and Selectivity				
ALK2 IC ₅₀ (nM)	<20	13	7	19
ALK2 ^{G328V/R206H/R258G} IC ₅₀ (nM)	<20	8, 9, 13	-	-
ALK5 IC ₅₀ (nM)	>1000	2427	>5000	2206
ALK2 NanoBRET IC ₅₀ (nM)	<100	45	29	98
ALK2 ^{G328V/G356D/Q207D/R206H} NanoBRET IC ₅₀ (nM)	<100	6, 16, 7, 12	-	-
ALK5 DLA/ALK2 NanoBRET	>30	45	115	74
DIPG-XXI and -007 Cell Line GI ₅₀ (nM)	<500	52, 130	28, 2095	214, 36
Kinome-wide Selectivity (ex ALK1-6)	Number w/ >50% inhibition @ 1 μM	8/368	7/368	13/368
In Vitro ADME				
MLM (% @ 1 h)	>50	65	56	66
HLM (% @ 1 h)	>50	71	71	84
Caco-2 P _{app,AB} (× 10 ⁻⁶ cm/sec)	>3	5.4	9.7	1.8 ^a
Caco-2 BA/AB	<2.0	1.5	0.8	2.7
CYP (7 isoforms) IC ₅₀ (μM)	>10	>10	>10	>10 ^b
hERG IC ₅₀ (μM)	>10	8.3	4.8	2.5
Ames	Negative	Negative	-	-
In Vivo ADME/PK (Mice)^c				
Cl (mL/min/kg)	<30	12.7	8.90	17.1
V _{ss} (L/kg)	>1	2.05	2.44	2.77
t _{1/2} (h)	>3	3.11	3.67	3.68
C _{max} (μM)	>1	6.16	4.74	3.19
F (%)	>50	100	74	95
Dose/Exposure	Linear @ 10-100 mg/kg PO (r > 0.95)	Yes	Yes	Yes
C _{brain} /C _{plasma} (B/P) @ 4 h	>0.5	0.90*	0.82	1.41

^aLow post-assay recovery. ^b2C9 IC₅₀ = 7.3 μM and 2C19 IC₅₀ = 7.7 μM. ^c2 mg/kg IV and 10 mg/kg PO dosing.

compounds as suitable inhibitors for proof-of-concept *in vivo* studies in models of FOP and DIPG. Active against ALK2^{R206H}

in vitro, we anticipated that explicit *in vivo* target engagement could be demonstrated with 14 day compound dosing in an

injury-induced heterotopic ossification (HO) *Acvr1*^{R206H/+} mouse model of FOP.⁶³ Efficacy in this model would build confidence to dose compounds over 28–56 days in an orthotopic H3.1K27M, *ACVR1*^{R206H} (Cre, PDGFA infected),²⁷ or patient-derived H3.3K27M, *ACVR1*^{R206H} HSJD-DIPG-007 tumor xenograft⁴³ mouse model of DIPG. Full disclosure of the *in vitro* biology and *in vivo* model outcomes is beyond the scope of this publication and will be done under separate cover (see the Supporting Information, Note S2).

CONCLUSIONS

With the recent identification of ALK2 as a suitable target for therapeutic intervention in the treatment of DIPG, inhibitors from several chemical classes have been reported (Figure 1). One of the most well characterized, LDN-214117, demonstrated significant efficacy in an orthotopic mouse model of the disease and provided the basis for the further development of related inhibitors.⁴³ In this work, using LDN-214117 as a lead compound, we expanded the SAR around the 3,5-diphenylpyridine inhibitor class to optimize potency against ALK2, increase selectivity over important off-targets such as ALK5, and produce a set of preclinical compounds with superior ADME and PK properties characteristic of a viable CNS drug. With the development of compound 6a, we found that incorporation of a C-4 position methyl group on the pyridine core allowed for greater potency against ALK2 in both biochemical and cell-based assays while simultaneously conferring increased selectivity over ALK5. The compound also exhibited remarkable kinome-wide selectivity, little activity against other (receptor) off-targets, no significant CYP inhibition, and a manageable degree of activity against the hERG potassium channel. Subsequent structural modifications at the C-3 and C-5 positions gave rise to compounds 11b and 14k, which not only possessed the favorable PK characteristics evident in 6a but also demonstrated the superior levels of BBB penetration required of a CNS drug candidate. The aggregate properties of 6a, 11b, and 14k prompted us to select these compounds for further preclinical development as advanced candidates M4K2009, M4K2163, and M4K2117, respectively. All three inhibitors satisfied the criteria of our target product profile (TPP), with only hERG potassium channel inhibition being the exception (Table 6).

Employing an open science model, we were able to compress the development timeline for these analogs by bringing together chemistry and biological screening capacity. Extensive evaluation of M4K2009, M4K2117, and M4K2163 *in vitro* against patient-derived DIPG cell lines and *in vivo* proof-of-concept studies in orthotopic mouse models of DIPG will be conducted in an equally open manner, with complete results to be reported at a later date.

EXPERIMENTAL SECTION

Chemistry. All reagents were purchased from commercial vendors and used without further purification. Volatiles were removed under reduced pressure by rotary evaporation or using the V-10 solvent evaporator system from Biotage. Very high boiling point (6000 rpm, 0 mbar, 56 °C), mixed volatile (7000 rpm, 30 mbar, 36 °C), and volatile (6000 rpm, 30 mbar, 36 °C) methods were used to evaporate solvents. The yields given refer to chromatographically purified and spectroscopically pure compounds, unless stated otherwise. Compounds were purified using a Biotage Isolera One system by normal phase chromatography using Biotage SNAP KP-Sil or Sfar Silica D columns (part no. FSKO-1107/FSRD-0445) or by reverse-phase chromatography using Biotage SNAP KP-C18-HS or Sfar C18 D

columns (part no. FSLO-1118/FSUD-040). If additional purification was required, compounds were purified by solid-phase extraction (SPE) using Biotage Isolute Flash SCX-2 cation exchange cartridges (part nos. 532-0050-C and 456-0200-D). Products were washed with two cartridge volumes of MeOH and eluted with a solution of MeOH and NH₄OH (9:1 v/v). Preparative chromatography was carried out using a Waters 2767 injector with a collector attached to PDA UV–vis and SQD mass detectors. An XSelect CSH Prep C18 5 μm OBD 19 mm × 100 mm (part no. 186005421) or an Xselect CSH Prep C18 5 μm 10 mm × 100 mm (part no. 186005415) column was used for purification. Final compounds were dried using the Labconco Benchtop Freeze-Zone™ Freeze-Dry System (4.5 L model). ¹H NMRs were recorded on a Bruker Avance-III 500 MHz spectrometer at ambient temperature. Residual protons of CDCl₃, DMSO-*d*₆, and CD₃OD solvents were used as internal references. Spectral data are reported as follows: chemical shift (δ in ppm), multiplicity (br, broad; s, singlet; d, doublet; dd, doublet of doublets; m, multiplet), coupling constants (*J* in Hz), and proton integration. Compound purity was determined by UV absorbance at 254 nm during tandem liquid chromatography/mass spectrometry (LCMS) using a Waters Acquity separation module. All final compounds had a purity of $\geq 95\%$ as determined using this method. Low-resolution mass spectrometry was conducted in the positive ion mode using a Waters Acquity SQD mass spectrometer (electrospray ionization source) fitted with a PDA detector. Mobile phase A consisted of 0.1% formic acid in water, while mobile phase B consisted of 0.1% formic acid in acetonitrile. One of three types of columns were used; column 1: Acquity UPLC CSH C18 (2.1 mm × 50 mm, 130 Å, 1.7 μm, part no. 186005296); column 2: Acquity UPLC BEH C8 (2.1 mm × 50 mm, 130 Å, 1.7 μm, part no. 186002877); or column 3: Acquity UPLC HSS T3 (2.1 mm × 50 mm, 100 Å, 1.8 μm, part no. 186003538). For columns 1 and 2, the gradient went from 90 to 5% mobile phase A over 1.8 min, maintained at 5% for 0.5 min, then increased to 90% over 0.2 min for a total run time of 3 min. For column 3, the gradient went from 98 to 5% mobile phase A over 1.8 min, maintained at 5% for 0.5 min, then increased to 98% over 0.2 min for a total run time of 3 min. The flow rate was 0.4 mL/min throughout both runs. All columns were used with the temperature maintained at 25 °C. High-resolution mass spectrometry was conducted using a Waters Synapt G2-S quadrupole-time-of-flight (Q-TOF) hybrid mass spectrometer system coupled with an Acquity ultraperformance liquid chromatography (UPLC) I-Class system. Chromatographic separations were carried out on an Acquity UPLC HSS T3 (2.1 mm × 100 mm, 100 Å, 1.8 μm, part no. 186003539). The mobile phases were 0.1% formic acid in water (solvent A) and 0.1% formic acid in acetonitrile (solvent B). Leucine Enkephalin was used as the lock-mass. MassLynx 4.1 was used for data analysis.

General Procedure A for the Synthesis of Intermediates 3a, 3d–e, and 3g–i. To a solution of 3-bromo-5-chloro-pyridine 1a, 1d–e, or 1g–i (0.484 mmol), 3,4,5-trimethoxyphenylboronic acid (2) (103 mg, 0.484 mmol), and Na₂CO₃ (205 mg, 1.94 mmol) in DMF (2.2 mL) and water (0.6 mL) at room temperature was added [1,12-bis-(diphenylphosphino)ferrocene]dichloropalladium(II)·DCM complex (20 mg, 0.024 mmol). After heating the resulting mixture at 100 °C for 16 h, it was cooled down to room temperature and diluted with water (40 mL) and the aqueous layer was extracted with EtOAc (3 × 20 mL). The combined organic extracts were dried with anhydrous Na₂SO₄, filtered, and concentrated under reduced pressure. This crude material was purified by chromatography on silica (10–100% EtOAc in hexanes) to afford intermediate 3a, 3e, 3h–i (all in >70% yield), 3d, or 3g (both in ~50% yield) as a powder. The identity of all products was confirmed by low-resolution mass spectrometry (LRMS) before use in the subsequent synthetic step.

General Procedure B for the Synthesis of Intermediates 3b–c and 3f. To a solution of 3,5-dichloropyridine 1b–c or 1f (0.484 mmol), 3,4,5-trimethoxyphenylboronic acid (2) (103 mg, 0.484 mmol), and XPhos Pd G2 (19 mg, 0.024 mmol) in butanol (3 mL) at room temperature was added K₃PO₄ (1.3 M solution in water) (0.748 mL, 0.973 mmol). After heating the resulting mixture at 100 °C for 4 h, it was cooled down to room temperature and diluted with water (40 mL) and the aqueous layer was extracted with EtOAc (3 × 20 mL). The

combined organic extracts were dried with anhydrous Na_2SO_4 , filtered, and concentrated under reduced pressure. This crude material was purified by chromatography on silica (10–100% EtOAc in hexanes) to afford intermediate **3b–c** or **3f** (all in ~50% yield) as a powder. The identity of all products was confirmed by LRMS before use in the subsequent synthetic step.

Procedure for the Synthesis of Intermediates 5a–i. General procedure B, with *tert*-butyl 4-[4-(4,4,5,5-tetramethyl-1,3,2-dioxaborolan-2-yl)phenyl]piperazine-1-carboxylate (**4**) replacing 3,4,5-trimethoxyphenylboronic acid (**2**), was used to synthesize intermediates **5a–i** (all in >70% yield) as a powder from intermediates **3a–i**. The identity of all products was confirmed by LRMS before use in the subsequent synthetic step.

General Procedure C for the Synthesis of Compounds 6a–i. To a solution of intermediates **5a–i** (0.230 mmol) in methanol (MeOH) (4 mL) at room temperature was added hydrogen chloride solution (4.0 M in dioxane) (0.29 mL, 1.16 mmol). The resulting mixture was stirred for 30 min prior to removal of all solvents under reduced pressure, dissolution of the residue in a minimal amount of MeOH, and purification by SPE to afford compounds **6a–i** (all in >95% yield) as a powder.

1-(4-(4-Methyl-5-(3,4,5-trimethoxyphenyl)pyridin-3-yl)phenyl)piperazine (6a) (M4K2009). $^1\text{H NMR}$ (500 MHz, MeOD- d_4) δ 8.32 (s, 1H), 8.31 (s, 1H), 7.33 (d, $J = 8.9$ Hz, 2H), 7.12 (d, $J = 8.8$ Hz, 2H), 6.70 (s, 2H), 3.90 (s, 6H), 3.86 (s, 3H), 3.28–3.24 (m, 4H), 3.07–3.03 (m, 4H), 2.26 (s, 3H). HRMS (ESI) for $\text{C}_{25}\text{H}_{30}\text{N}_3\text{O}_3$ [$\text{M} + \text{H}$] $^+$ m/z : calcd, 420.2287; found, 420.2279.

1-(4-(4-Ethyl-5-(3,4,5-trimethoxyphenyl)pyridin-3-yl)phenyl)piperazine (6b). $^1\text{H NMR}$ (500 MHz, MeOD- d_4) δ 8.29 (s, 1H), 8.25 (s, 1H), 7.31 (d, $J = 8.5$ Hz, 2H), 7.14 (d, $J = 8.5$ Hz, 2H), 6.68 (s, 2H), 3.88 (s, 6H), 3.84 (s, 3H), 3.40–3.36 (m, 4H), 3.25–3.21 (m, 4H), 2.75–2.68 (m, 2H), 0.82 (t, $J = 7.5$ Hz, 3H). HRMS (ESI) for $\text{C}_{26}\text{H}_{32}\text{N}_3\text{O}_3$ [$\text{M} + \text{H}$] $^+$ m/z : calcd, 434.2444; found, 434.2436.

1-(4-(4-Cyclopropyl-5-(3,4,5-trimethoxyphenyl)pyridin-3-yl)phenyl)piperazine (6c). $^1\text{H NMR}$ (500 MHz, MeOD- d_4) δ 8.44 (s, 1H), 8.42 (s, 1H), 7.52 (d, $J = 8.5$ Hz, 2H), 7.19 (d, $J = 8.5$ Hz, 2H), 6.89 (s, 2H), 3.98 (s, 6H), 3.93 (s, 3H), 3.37 (d, $J = 4.9$ Hz, 4H), 3.21–3.14 (m, 4H), 2.32–2.20 (m, 1H), 0.63–0.58 (br m, 2H), 0.05–0.00 (br m, 2H). HRMS (ESI) for $\text{C}_{27}\text{H}_{32}\text{N}_3\text{O}_3$ [$\text{M} + \text{H}$] $^+$ m/z : calcd, 446.2444; found, 446.2437.

1-(4-(4-Methoxy-5-(3,4,5-trimethoxyphenyl)pyridin-3-yl)phenyl)piperazine (6d). $^1\text{H NMR}$ (500 MHz, CDCl_3 - d_1) δ 8.49 (s, 1H), 8.46 (s, 1H), 7.49 (d, $J = 8.8$ Hz, 2H), 7.02 (d, $J = 8.8$ Hz, 2H), 6.79 (s, 2H), 3.94–3.88 (m, 9H), 3.39 (s, 3H), 3.28–3.21 (m, 4H), 3.12–3.04 (m, 4H). HRMS (ESI) for $\text{C}_{25}\text{H}_{30}\text{N}_3\text{O}_4$ [$\text{M} + \text{H}$] $^+$ m/z : calcd, 436.2236; found, 436.2234.

3-(4-(Piperazin-1-yl)phenyl)-5-(3,4,5-trimethoxyphenyl)pyridin-4-amine (6e). $^1\text{H NMR}$ (500 MHz, MeOD- d_4) δ 7.85 (s, 1H), 7.82 (s, 1H), 7.25 (d, $J = 8.7$ Hz, 2H), 7.01 (d, $J = 8.7$ Hz, 2H), 6.64 (s, 2H), 3.78 (s, 6H), 3.72 (s, 3H), 3.15–3.08 (m, 4H), 2.94–2.87 (m, 4H). HRMS (ESI) for $\text{C}_{24}\text{H}_{29}\text{N}_4\text{O}_3$ [$\text{M} + \text{H}$] $^+$ m/z : calcd, 421.2240; found, 421.2235.

1-(4-(4-Fluoro-5-(3,4,5-trimethoxyphenyl)pyridin-3-yl)phenyl)piperazine (6f). $^1\text{H NMR}$ (500 MHz, MeOD- d_4) δ 8.59 (d, $J = 5.4$ Hz, 1H), 8.57 (d, $J = 5.4$ Hz, 1H), 7.57 (d, $J = 7.8$ Hz, 2H), 7.14 (d, $J = 8.8$ Hz, 2H), 6.91 (s, 2H), 3.91 (s, 6H), 3.85 (s, 3H), 3.40–3.36 (m, 4H), 3.22–3.16 (m, 4H). HRMS (ESI) for $\text{C}_{24}\text{H}_{27}\text{FN}_3\text{O}_3$ [$\text{M} + \text{H}$] $^+$ m/z : calcd, 424.2036; found, 424.2025.

1-(4-(4-Chloro-5-(3,4,5-trimethoxyphenyl)pyridin-3-yl)phenyl)piperazine (6g). $^1\text{H NMR}$ (500 MHz, DMSO- d_6) δ 8.52 (s, 1H), 8.48 (s, 1H), 7.39 (d, $J = 8.2$ Hz, 2H), 7.03 (d, $J = 8.3$ Hz, 2H), 6.82 (s, 2H), 3.82 (s, 6H), 3.72 (s, 3H), 3.14 (br s, 4H), 2.85 (br s, 4H). HRMS (ESI) for $\text{C}_{24}\text{H}_{27}\text{ClN}_3\text{O}_3$ [$\text{M} + \text{H}$] $^+$ m/z : calcd, 440.1741; found, 440.1728.

1-(4-(4-(Trifluoromethyl)-5-(3,4,5-trimethoxyphenyl)pyridin-3-yl)phenyl)piperazine (6h). $^1\text{H NMR}$ (500 MHz, MeOD- d_4) δ 8.60 (s, 1H), 8.56 (s, 1H), 7.33 (d, $J = 8.7$ Hz, 2H), 7.09 (d, $J = 8.8$ Hz, 2H), 6.74 (s, 2H), 3.89 (s, 6H), 3.85 (s, 3H), 3.28–3.24 (m, 4H), 3.05–3.01 (m, 4H). HRMS (ESI) for $\text{C}_{25}\text{H}_{27}\text{F}_3\text{N}_3\text{O}_3$ [$\text{M} + \text{H}$] $^+$ m/z : calcd, 474.2005; found, 474.2000.

3-(4-(Piperazin-1-yl)phenyl)-5-(3,4,5-trimethoxyphenyl)isonicotinonitrile (6i). $^1\text{H NMR}$ (500 MHz, MeOD- d_4) δ 8.76 (s, 1H),

8.75 (s, 1H), 7.62 (d, $J = 8.7$ Hz, 2H), 7.16 (d, $J = 8.7$ Hz, 2H), 7.00 (s, 2H), 3.95 (s, 6H), 3.88 (s, 3H), 3.35–3.31 (m, 4H), 3.07–3.03 (m, 4H). HRMS (ESI) for $\text{C}_{25}\text{H}_{27}\text{N}_4\text{O}_3$ [$\text{M} + \text{H}$] $^+$ m/z : calcd, 431.2083; found, 431.2074.

Procedure for the Synthesis of Intermediates 7a–b. General procedure A, with *tert*-butyl 4-[4-(4,4,5,5-tetramethyl-1,3,2-dioxaborolan-2-yl)phenyl]piperazine-1-carboxylate (**4**) replacing 3,4,5-trimethoxyphenylboronic acid (**2**), was used to synthesize intermediates **7a–b** (both in >70% yield) as a powder from 3-bromo-5-chloro-pyridine **1a** or **1i**. The identity of both products was confirmed by LRMS before use in the subsequent synthetic step.

Procedure for the Synthesis of Intermediates 10a–c. General procedure B, with either 3,5-dimethoxyphenylboronic acid (**8**) or (4-fluoro-3,5-dimethoxyphenyl)boronic acid (**9**) replacing 3,4,5-trimethoxyphenylboronic acid (**2**), was used to synthesize intermediates **10a–c** (all in >70% yield) as a powder from intermediates **7a–b**. The identity of all products was confirmed by LRMS before use in the subsequent synthetic step.

Procedure for the Synthesis of Compounds 11a–c. General procedure C, with intermediates **10a–c** replacing intermediates **5a–i**, was used to synthesize compounds **11a–c** (all in >95% yield) as a powder.

1-(4-(5-(3,5-Dimethoxyphenyl)-4-methylpyridin-3-yl)phenyl)piperazine (11a). $^1\text{H NMR}$ (500 MHz, MeOD- d_4) δ 8.18 (s, 1H), 8.16 (s, 1H), 7.20 (d, $J = 8.7$ Hz, 2H), 6.99 (d, $J = 8.7$ Hz, 2H), 6.45 (t, $J = 2.1$ Hz, 1H), 6.41 (d, $J = 2.2$ Hz, 2H), 3.72 (s, 6H), 3.20–3.15 (m, 4H), 3.04–2.93 (m, 4H), 2.10 (s, 3H). HRMS (ESI) for $\text{C}_{24}\text{H}_{28}\text{N}_3\text{O}_2$ [$\text{M} + \text{H}$] $^+$ m/z : calcd, 390.2182; found, 390.2171.

1-(4-(5-(4-Fluoro-3,5-dimethoxyphenyl)-4-methylpyridin-3-yl)phenyl)piperazine (11b) (M4K2163). $^1\text{H NMR}$ (500 MHz, MeOD- d_4) δ 8.32 (s, 2H), 7.32 (d, $J = 8.8$ Hz, 2H), 7.12 (d, $J = 8.8$ Hz, 2H), 6.75 (d, $J = 7.0$ Hz, 2H), 3.92 (s, 6H), 3.28–3.23 (m, 4H), 3.07–3.02 (m, 4H), 2.25 (s, 3H). HRMS (ESI) for $\text{C}_{24}\text{H}_{27}\text{FN}_3\text{O}_2$ [$\text{M} + \text{H}$] $^+$ m/z : calcd, 408.2087; found, 408.2075.

3-(4-Fluoro-3,5-dimethoxyphenyl)-5-(4-(piperazin-1-yl)phenyl)isonicotinonitrile (11c). $^1\text{H NMR}$ (500 MHz, MeOD- d_4) δ 8.65 (s, 1H), 8.63 (s, 1H), 7.51 (d, $J = 8.8$ Hz, 2H), 7.06 (s, 1H), 7.04 (s, 1H), 6.93 (d, $J = 6.9$ Hz, 2H), 3.84 (s, 6H), 3.26–3.21 (m, 4H), 3.01–2.96 (m, 4H). HRMS (ESI) for $\text{C}_{24}\text{H}_{24}\text{FN}_4\text{O}_2$ [$\text{M} + \text{H}$] $^+$ m/z : calcd, 419.1883; found, 419.1874.

Procedure for the Synthesis of Intermediates 13c, 13j, 13l, 13n, and 13p and Compounds 14a–b, 14h–i, 14k, 14m, 14o, and 14q. General procedure B, with a 4-(R_1)phenylboronic acid/pinacol ester **12a–c** or **12h–q** replacing 3,4,5-trimethoxyphenylboronic acid (**2**), was used to synthesize intermediates **13c, 13j, 13l, 13n, or 13p** and compound **14a–b, 14h–i, 14k, 14m, 14o, or 14q** (all in >70% yield) as a powder from intermediate **3a**.

Procedure for the Synthesis of Compounds 14c, 14j, 14l, 14n, and 14p. General procedure C, with intermediate **13c, 13j, 13l, 13n, or 13p** replacing intermediates **5a–i**, was used to synthesize compound **14c, 14j, 14l, 14n, or 14p** (all in >95% yield) as a powder.

Procedure for the Synthesis of Compound 14d. To a solution of compound **6a** (M4K2009) (40 mg, 0.095 mmol) and 2-fluoroethyl tosylate (25 mg, 0.114 mmol) in acetonitrile (1 mL) at room temperature was added TEA (19 mg, 0.190 mmol). After heating the resulting mixture at 100 °C for 16 h, it was cooled down to room temperature and diluted with water (30 mL) and the aqueous layer was extracted with EtOAc (3 × 20 mL). The combined organic extracts were dried with anhydrous Na_2SO_4 , filtered, and concentrated under reduced pressure. This crude material was purified by chromatography on silica (0–20% MeOH in EtOAc) to afford compound **14d** (65% yield) as a powder.

General Procedure for the Synthesis of Compounds 14e–g. To a solution of compound **6a** (M4K2009) (40 mg, 0.095 mmol) in THF (4 mL) at room temperature was added acetyl chloride (for **14e**), dimethylcarbonyl chloride (for **14f**), or methanesulfonyl chloride (for **14g**) (0.114 mmol) and DIPEA (25 mg, 0.190 mmol). After stirring the resulting mixture for 1 h, it was diluted with water (30 mL) and the aqueous layer was extracted with EtOAc (3 × 20 mL). The combined organic extracts were dried with anhydrous Na_2SO_4 , filtered, and

concentrated under reduced pressure. This crude material was purified by chromatography on silica (0–100% EtOAc in hexanes) to afford compounds **14e–g** (all in >80% yield) as a powder.

1-Methyl-4-(4-(4-methyl-5-(3,4,5-trimethoxyphenyl)pyridin-3-yl)phenyl)piperazine (14a). ¹H NMR (500 MHz, MeOD-*d*₄) δ 8.30 (d, *J* = 2.7 Hz, 2H), 7.31 (t, *J* = 5.7 Hz, 2H), 7.11 (d, *J* = 8.8 Hz, 2H), 6.69 (s, 2H), 3.89 (s, 6H), 3.84 (s, 3H), 3.33–3.29 (m, 4H), 2.72–2.67 (m, 4H), 2.41 (s, 3H), 2.24 (s, 3H). HRMS (ESI) for C₂₆H₃₂N₃O₃ [M + H]⁺ *m/z*: calcd, 434.2444; found, 434.2432.

1-Isopropyl-4-(4-(4-methyl-5-(3,4,5-trimethoxyphenyl)pyridin-3-yl)phenyl)piperazine (14b). ¹H NMR (500 MHz, MeOD-*d*₄) δ 8.31 (s, 2H), 7.32 (d, *J* = 8.7 Hz, 2H), 7.11 (d, *J* = 8.7 Hz, 2H), 6.69 (s, 2H), 3.89 (s, 6H), 3.84 (s, 3H), 3.33–3.29 (m, 4H), 2.84–2.68 (m, 5H), 2.25 (s, 3H), 1.17 (d, *J* = 6.5 Hz, 6H). HRMS (ESI) for C₂₈H₃₆N₃O₃ [M + H]⁺ *m/z*: calcd, 462.2757; found, 462.2746.

(3S,5R)-3,5-Dimethyl-1-(4-(4-methyl-5-(3,4,5-trimethoxyphenyl)pyridin-3-yl)phenyl)piperazine (14c). ¹H NMR (500 MHz, DMSO-*d*₆) δ 8.35 (s, 1H), 8.32 (s, 1H), 7.28 (br d, *J* = 8.6 Hz, 2H), 7.02 (br d, *J* = 8.7 Hz, 2H), 6.72 (s, 2H), 3.81 (s, 6H), 3.72 (s, 3H), 3.61 (br d, *J* = 10.8 Hz, 2H), 2.80–2.90 (m, 2H), 2.10–2.20 (m, 6H), 1.04 (d, *J* = 6.2 Hz, 6H). HRMS (ESI) for C₂₇H₃₄N₃O₃ [M + H]⁺ *m/z*: calcd, 448.2600; found, 448.2591.

1-(2-Fluoroethyl)-4-(4-(4-methyl-5-(3,4,5-trimethoxyphenyl)pyridin-3-yl)phenyl)piperazine (14d). ¹H NMR (500 MHz, MeOD-*d*₄) δ 8.18 (s, 2H), 7.19 (d, *J* = 8.6 Hz, 2H), 6.99 (d, *J* = 8.6 Hz, 2H), 6.57 (s, 2H), 4.58 (t, *J* = 4.7 Hz, 1H), 4.49 (t, *J* = 4.9 Hz, 1H), 3.77 (s, 6H), 3.72 (s, 3H), 3.21–3.17 (m, 4H), 2.75–2.69 (m, 1H), 2.69–2.62 (m, 5H), 2.13 (s, 3H). HRMS (ESI) for C₂₇H₃₃FN₃O₃ [M + H]⁺ *m/z*: calcd, 466.2506; found, 466.2495.

1-(4-(4-(4-Methyl-5-(3,4,5-trimethoxyphenyl)pyridin-3-yl)phenyl)piperazin-1-yl)ethan-1-one (14e). ¹H NMR (500 MHz, DMSO-*d*₆) δ 8.37 (s, 1H), 8.34 (s, 1H), 7.33 (br d, *J* = 8.3 Hz, 2H), 7.07 (br d, *J* = 8.6 Hz, 2H), 6.73 (s, 2H), 3.82 (s, 6H), 3.72 (s, 3H), 3.60 (br s, 4H), 3.25 (br s, 2H), 3.18 (br s, 2H), 2.19 (s, 3H), 2.06 (s, 3H). HRMS (ESI) for C₂₇H₃₂N₃O₄ [M + H]⁺ *m/z*: calcd, 462.2393; found, 462.2391.

***N,N*-Dimethyl-4-(4-(4-methyl-5-(3,4,5-trimethoxyphenyl)pyridin-3-yl)phenyl)piperazine-1-carboxamide (14f).** ¹H NMR (500 MHz, DMSO-*d*₆) δ 8.37 (s, 1H), 8.34 (s, 1H), 7.33 (d, *J* = 8.6 Hz, 2H), 7.08 (d, *J* = 8.7 Hz, 2H), 6.73 (s, 2H), 3.82 (s, 6H), 3.72 (s, 3H), 3.28 (br d, *J* = 6.1 Hz, 4H), 3.23 (br d, *J* = 5.7 Hz, 4H), 2.80 (s, 6H), 2.19 (s, 3H). HRMS (ESI) for C₂₈H₃₅N₄O₄ [M + H]⁺ *m/z*: calcd, 491.2658; found, 491.2652.

1-(4-(4-Methyl-5-(3,4,5-trimethoxyphenyl)pyridin-3-yl)phenyl)-4-(methylsulfonyl)piperazine (14g). ¹H NMR (500 MHz, MeOD-*d*₄) δ 8.32 (s, 1H), 8.30 (s, 1H), 7.34 (d, *J* = 8.7 Hz, 2H), 7.15 (d, *J* = 8.7 Hz, 2H), 6.69 (s, 2H), 3.89 (s, 6H), 3.84 (s, 3H), 3.44–3.37 (m, 8H), 2.92 (s, 3H), 2.44 (s, 3H). HRMS (ESI) for C₂₆H₃₂N₃O₅S [M + H]⁺ *m/z*: calcd, 498.2063; found, 498.2049.

4-(4-(4-Methyl-5-(3,4,5-trimethoxyphenyl)pyridin-3-yl)phenyl)morpholine (14h). ¹H NMR (500 MHz, DMSO-*d*₆) δ 8.35 (s, 1H), 8.33 (s, 1H), 7.32 (br d, *J* = 8.1 Hz, 2H), 7.06 (br d, *J* = 8.2 Hz, 2H), 6.73 (s, 2H), 3.82 (s, 6H), 3.76 (br d, *J* = 4.0 Hz, 4H), 3.72 (s, 3H), 3.18 (br d, *J* = 4.2 Hz, 4H), 2.19 (s, 3H). HRMS (ESI) for C₂₅H₂₉N₂O₄ [M + H]⁺ *m/z*: calcd, 421.2127; found, 421.2123.

4-(4-(4-Methyl-5-(3,4,5-trimethoxyphenyl)pyridin-3-yl)phenyl)thiomorpholine 1,1-Dioxide (14i). ¹H NMR (500 MHz, DMSO-*d*₆) δ 8.37 (s, 1H), 8.34 (s, 1H), 7.35 (br d, *J* = 8.6 Hz, 2H), 7.15 (br d, *J* = 8.7 Hz, 2H), 6.73 (s, 2H), 3.85 (br s, 4H), 3.82 (s, 6H), 3.72 (s, 3H), 3.16 (br s, 4H), 2.20 (s, 3H). HRMS (ESI) for C₂₅H₂₉N₂O₅S [M + H]⁺ *m/z*: calcd, 469.1797; found, 469.1793.

4-Methyl-3-(4-(4-(piperidin-4-yl)phenyl)-5-(3,4,5-trimethoxyphenyl)pyridine (14j). ¹H NMR (500 MHz, MeOD-*d*₄) δ 8.36 (s, 1H), 8.30 (s, 1H), 7.42 (q, *J* = 8.3 Hz, 4H), 6.70 (s, 2H), 3.89 (s, 6H), 3.84 (s, 3H), 3.45 (d, *J* = 12.8 Hz, 2H), 3.08 (td, *J* = 12.7, 2.3 Hz, 2H), 2.96 (ddd, *J* = 12.1, 8.8, 3.5 Hz, 1H), 2.23 (s, 3H), 2.10 (d, *J* = 13.8 Hz, 2H), 1.92 (qd, *J* = 13.5, 3.8 Hz, 2H). HRMS (ESI) for C₂₆H₃₁N₂O₃ [M + H]⁺ *m/z*: calcd, 419.2335; found, 419.2330.

4-Methyl-3-(4-(1-methylpiperidin-4-yl)phenyl)-5-(3,4,5-trimethoxyphenyl)pyridine (14k) (M4K2117). ¹H NMR (500 MHz, MeOD-*d*₄) δ 8.35 (s, 1H), 8.31 (s, 1H), 7.42 (d, *J* = 8.2 Hz, 2H), 7.37

(d, *J* = 8.2 Hz, 2H), 6.70 (s, 2H), 3.90 (s, 6H), 3.85 (s, 3H), 3.08 (d, *J* = 11.7 Hz, 2H), 2.72–2.63 (m, 1H), 2.40 (s, 3H), 2.30–2.23 (m, 2H), 2.23 (br s, 3H), 1.95–1.86 (m, 4H). HRMS (ESI) for C₂₇H₃₃N₂O₃ [M + H]⁺ *m/z*: calcd, 433.2491; found, 433.2485.

4-Methyl-3-(4-(1,2,3,6-tetrahydropyridin-4-yl)phenyl)-5-(3,4,5-trimethoxyphenyl)pyridine (14l). ¹H NMR (500 MHz, MeOD-*d*₄) δ 8.23 (s, 1H), 8.20 (s, 1H), 7.47 (d, *J* = 8.3 Hz, 2H), 7.28 (d, *J* = 8.3 Hz, 2H), 6.58 (s, 2H), 6.20–6.13 (m, 1H), 3.77 (s, 6H), 3.72 (s, 3H), 3.46 (dd, *J* = 5.6, 2.6 Hz, 2H), 3.05 (t, *J* = 5.8 Hz, 2H), 2.54–2.46 (m, 2H), 2.12 (s, 3H). HRMS (ESI) for C₂₆H₂₉N₂O₃ [M + H]⁺ *m/z*: calcd, 417.2178; found, 417.2172.

4-Methyl-3-(4-(1-methyl-1,2,3,6-tetrahydropyridin-4-yl)phenyl)-5-(3,4,5-trimethoxyphenyl)pyridine (14m). ¹H NMR (500 MHz, MeOD-*d*₄) δ 8.35 (s, 1H), 8.33 (s, 1H), 7.60 (d, *J* = 8.2 Hz, 2H), 7.41 (d, *J* = 8.2 Hz, 2H), 6.70 (s, 2H), 6.26 (s, 1H), 3.89 (s, 6H), 3.84 (s, 3H), 3.28 (d, *J* = 2.0 Hz, 2H), 2.86 (t, *J* = 5.7 Hz, 2H), 2.73 (s, 2H), 2.50 (s, 3H), 2.24 (s, 3H). HRMS (ESI) for C₂₇H₃₁N₂O₃ [M + H]⁺ *m/z*: calcd, 431.2335; found, 431.2328.

1-(4-(4-Methyl-5-(3,4,5-trimethoxyphenyl)pyridin-3-yl)phenyl)-1,4-diazepane (14n). ¹H NMR (500 MHz, DMSO-*d*₆) δ 8.33 (s, 2H), 7.24 (d, *J* = 8.7 Hz, 2H), 6.80 (d, *J* = 8.8 Hz, 2H), 6.73 (s, 2H), 3.81 (s, 6H), 3.72 (s, 3H), 3.57 (t, *J* = 6.0 Hz, 2H), 3.54–3.49 (m, 2H), 2.95–2.87 (m, 2H), 2.73–2.66 (m, 2H), 2.21 (s, 3H), 1.86–1.78 (m, 2H). HRMS (ESI) for C₂₆H₃₂N₃O₃ [M + H]⁺ *m/z*: calcd, 434.2444; found, 434.2433.

1-Methyl-4-(4-(4-methyl-5-(3,4,5-trimethoxyphenyl)pyridin-3-yl)benzyl)piperazine (14o). ¹H NMR (500 MHz, MeOD-*d*₄) δ 8.35 (s, 1H), 8.31 (s, 1H), 7.50 (d, *J* = 7.9 Hz, 2H), 7.40 (d, *J* = 8.0 Hz, 2H), 6.70 (s, 2H), 3.89 (s, 6H), 3.84 (s, 3H), 3.65 (s, 2H), 2.83–2.43 (br s, 8H), 2.36 (s, 3H), 2.23 (s, 3H). HRMS (ESI) for C₂₇H₃₄N₃O₃ [M + H]⁺ *m/z*: calcd, 448.2600; found, 448.2592.

4-Methyl-3-(4-(piperidin-4-yloxy)phenyl)-5-(3,4,5-trimethoxyphenyl)pyridine (14p). ¹H NMR (500 MHz, MeOD-*d*₄) δ 8.34 (s, 1H), 8.31 (s, 1H), 7.37 (d, *J* = 8.7 Hz, 2H), 7.13 (d, *J* = 8.7 Hz, 2H), 6.70 (s, 2H), 4.72–4.66 (m, 1H), 3.90 (s, 6H), 3.85 (s, 3H), 3.32–3.26 (m, 2H), 3.04–2.98 (m, 2H), 2.24 (s, 3H), 2.19–2.12 (m, 2H), 1.95–1.87 (m, 2H). HRMS (ESI) for C₂₆H₃₁N₂O₄ [M + H]⁺ *m/z*: calcd, 435.2284; found, 435.2273.

4-Methyl-3-(4-(1-methylpiperidin-4-yl)oxy)phenyl)-5-(3,4,5-trimethoxyphenyl)pyridine (14q). ¹H NMR (500 MHz, MeOD-*d*₄) δ 8.21 (s, 1H), 8.19 (s, 1H), 7.23 (d, *J* = 8.7 Hz, 2H), 6.97 (d, *J* = 8.7 Hz, 2H), 6.58 (s, 2H), 4.46–4.37 (br m, 1H), 3.77 (s, 6H), 3.72 (s, 3H), 2.74–2.62 (br m, 2H), 2.41–2.30 (br m, 2H), 2.25 (s, 3H), 2.12 (s, 3H), 2.02–1.92 (br m, 2H), 1.81–1.72 (br m, 2H). HRMS (ESI) for C₂₇H₃₃N₂O₄ [M + H]⁺ *m/z*: calcd, 449.2440; found, 449.2429.

Kinase Assay. The biochemical potencies of all compounds were measured by Reaction Biology Corporation (Malvern, Pennsylvania). Compounds were tested against ALK1/ACVRL1, ALK2/ACVR1, ALK3/BMPRIα, ALK4/ACVR1β, ALKS/TGFβ-R1, and ALK6/BMPRIβ in a 10-dose IC₅₀ mode with a twofold serial dilution starting at 1 or 5 μM. Reactions were conducted at an ATP concentration of 10 μM and Casein concentration of 1 mg/mL. LDN-193189 was tested as a control in a 10-dose IC₅₀ mode with a threefold serial dilution starting at 10 μM. Reductions in enzymatic activity were determined relative to dimethyl sulfoxide (DMSO) controls.

Cell Culture and Transfection. HEK-293 cells were maintained in Dulbecco's modified Eagle's medium (DMEM, Gibco) supplemented with 10% fetal bovine serum (FBS) (Thermo Fisher) and penicillin/streptomycin (Thermo Fisher). HEK-293 cells were transfected with the protein expression or reporter constructs using FuGENE HD (Promega) according to the manufacturer's instructions. Briefly, DNA was diluted into phenol red-free Opti-MEM (Gibco) at a concentration of 10 μg/mL. Without coming in contact with the sides of the container, 3 μL of FuGENE HD was added for each microgram of DNA used. After thorough mixing by inversion, FuGENE HD/DNA complexes were allowed to form by incubation at room temperature for 20 min. The transfection mixture (1 part) was added to 20 parts of the HEK-293 cell suspension with a density of 200 000 cells per mL (volume/volume). HEK-293 cells were incubated in a humidified, 37 °C

incubator with 5% CO₂ for 24 h before they were used in the NanoBRET target engagement assay or dual luciferase reporter assay.

NanoBRET Target Engagement Assay. ALK2-C-terminal nanoluciferase fusion with a GSSG linker was encoded by the pFC32K vector (Promega). ALK2-nanoluciferase fusion construct (1 part) was mixed with 9 parts of Transfection Carrier DNA (mass/mass) (Promega). Transfected cells were trypsinized and resuspended in Opti-MEM at a density of 200 000 cells per mL. Cells (17 μ L) were dispensed into each well of a 384-well flat-bottom polypropylene plate (Greiner). Working solution (20 \times) of the target engagement tracer PBI-6908 (Promega) was prepared by diluting DMSO stock in tracer dilution buffer (12.5 mM HEPES pH 7.5, 31.25% PEG-400). Stocks (1000 \times) of test compounds in DMSO (Cell Signaling Technology) were diluted further in Opti-MEM for 10 \times working solutions. After the addition of 1 μ L of 20 \times target engagement tracer and 2 μ L of 10 \times working solutions, contents of the wells were thoroughly mixed by agitating the plate at 500 rpm for 1 min. Cells were incubated in a humidified, 37 $^{\circ}$ C incubator with 5% CO₂ for 2 h prior to bioluminescence resonance energy transfer (BRET) measurement. For BRET measurement, the NanoBRET NanoGlo Substrate and the Extracellular NanoLuc Inhibitor (Promega) were diluted 166 \times and 500 \times , respectively, in Opti-MEM to produce 3 \times working stock. A PHERAstar FSX microplate reader (BMG Labtech) with the LUM 610-LP 460-80 optical module was used to measure the intensity of dual emission. A measurement interval of 1 s and gain settings of 3600 and 1879 for 610 and 460 nm, respectively, were used. Milli-BRET units (mBU) were calculated by dividing the signal measured at 610 nm with the signal measured at 460 nm and multiplying by 1000. The apparent EC₅₀ values of test compounds were estimated using the [Inhibitor] *versus* response (three-parameter) nonlinear regression curve fitting function of GraphPad Prism 7.

Dual Luciferase Reporter Assay. CAGA-Luc and Renilla-luciferase constructs (a gift from Dr. Petra Knaus, Free University of Berlin) were used as reporters for ALK5 signaling and loading control, respectively. The CAGA-Luc construct (4 parts) was mixed with 1 part of Renilla-luciferase construct (mass/mass). Ten thousand transfected cells were seeded into each well of a 96-well plate (Corning). Some 24 h after transfection, the cells were incubated with 10 ng/mL TGF β 1 (Peprotech, 100-21-10) and test compounds simultaneously at the concentrations indicated in a humidified, 37 $^{\circ}$ C incubator with 5% CO₂. Another 24 h later, the cells were harvested, lysed, and processed for the measurement of luciferase activity using the Dual-Luciferase Reporter Assay System (Promega) according to the manufacturer's instructions. Briefly, the culture medium was aspirated completely, and cells were lysed in 50 μ L of 1 \times PLB with 300 rpm agitation for 30 min. The cell lysate (10 μ L) was dispensed into each well of a 384-well flat-bottom polypropylene plate (Greiner). The luminescent signal of firefly- and Renilla-luciferase activity was measured sequentially using a PHERAstar FS microplate reader (BMG Labtech) after the addition of 25 μ L of LARII and Stop & Glo, respectively. A measurement interval of 2 s and gain setting of 3600 were used. The firefly-luciferase signal was normalized to the cell number by division with the Renilla-luciferase signal. The relative luciferase unit (RLU) was obtained by further division with the signal from cells without TGF β stimulation. The apparent EC₅₀ values of test compounds were estimated using the [Inhibitor] *versus* response (three-parameter) nonlinear regression curve fitting function of GraphPad Prism 7.

Caco-2 Permeability Assay. Caco-2 cells (C2BBE1) were purchased from American Type Culture Collection (ATCC). Caco-2 cell cultures were routinely maintained in T-75 tissue culture flasks in DMEM containing 20% FBS, 0.1 mg/mL normocin, and 0.05 mg/mL gentamicin. These cells were seeded at a density of 40 000 cells per well on the 24-well poly(ethylene terephthalate) (PET) membrane (1.0 μ m pore size, 0.3 cm² surface area) insert plates. Cell monolayers were grown for 21 or 22 days at 37 $^{\circ}$ C with 5% CO₂ in a humidified incubator. The cell culture medium was replaced twice weekly during the cell growth period. Prior to beginning the permeability assay, cell monolayers were rinsed with Hank's balanced salt solution (HBSS) twice to remove the residual cell culture medium. The assay buffer comprised HBSS containing 10 mM HEPES and 15 mM glucose at pH

7.4. The dosing buffer contained 5 μ M metoprolol (positive control), 5 μ M atenolol (negative control), and 100 μ M Lucifer yellow in the assay buffer. The receiving buffer contained 1% bovine serum albumin (BSA) in the assay buffer. The concentration of the test compound was 5 μ M in the dosing buffer (final DMSO concentration was 0.1%). Digoxin at 10 μ M was utilized as a P-gp substrate control. For the apical to basolateral (A to B) permeability experiment, 0.25 mL of the dosing buffer was added to the apical chambers, and 1.0 mL of the receiving buffer was added to the basolateral chambers of the assay plate. For the basolateral to apical (B to A) permeability experiment, 0.25 mL of the receiving buffer was added to the apical chambers, and 1.0 mL of dosing buffer was added to the basolateral chambers of the assay plates. The assay plates were then incubated at 37 $^{\circ}$ C for 2 h on an orbital shaker at 65 rpm. Sample solutions were taken from the donor chambers (10 μ L) and receiver chambers (100 μ L) after the incubation period. For each sample, there were two technical replicates. The sample solutions from donor chambers were diluted 10 \times with the receiving buffer. To extract test compounds and precipitate BSA from sample solutions, three volumes of acetonitrile (containing 0.5% formic acid and an internal standard) were added, and the plate was vigorously mixed. Sample solutions were then centrifuged at 4000 rpm for 10 min to remove debris and precipitated BSA. Approximately 150 μ L of the supernatant was subsequently transferred to a new 96-well microplate for LC/MS analysis. Narrow-window mass extraction LC/MS analysis was performed for all samples using a Waters Acquity UPLC system with a Waters Xevo quadrupole-time-of-flight (Q-TOF) mass spectrometer to determine relative peak areas of the parent compounds. Chromatographic separations were performed on a Waters Acquity UPLC HSS T3 column (2.1 mm \times 100 mm, 100 \AA , 1.8 μ m, part no. 186003539) at 30 $^{\circ}$ C. Mobile phases A and B were 0.1% formic acid in water and 0.1% formic acid in acetonitrile, respectively. The sample temperature was kept at 10 $^{\circ}$ C. The typical injection volume was 0.3 μ L. Chromatographic gradients used are shown in the table below.

Time (min)	Flow Rate (μ L/min)	%A	%B
0.0	0.400	100	0
0.5	0.400	100	0
4.5	0.400	5	95
5.0	0.400	5	95
5.5	0.400	100	0
6.5	0.400	100	0

Data acquisition was performed in the electrospray (ES) positive ion mode in the mass range of 100–1000 *m/z*. The following source parameters were used: capillary voltage, 0.8 kV; cone voltage, 25 V; source temperature, 150 $^{\circ}$ C; desolvation temperature, 500 $^{\circ}$ C; cone gas flow, 150 L/h; desolvation gas flow, 600 L/h. Accurate masses were measured in the lock-spray automated exact mass measurement mode. The fragment ions of leucine-enkephalin were used as reference substances (lock-mass) in the acquisition mode. The following lock-spray configuration was used: frequency, 10 s; cone voltage, 25 V; collision energy, 22 V. Data processing was performed using MassLynx 4.1 software (Waters). The co-dosed positive and negative controls were also measured for each well to monitor integrity of cell monolayers and well-to-well variability. The apparent permeability coefficient (P_{app}) and post-assay recovery are calculated using the following equations

$$P_{app} = V_r \times (dC/dt) \times 1/(A \times C_0)$$

$$\text{percent recovery} = 100 \times [(V_r \times C_r^{\text{final}}) + (V_d \times C_d^{\text{final}})] / (V_d \times C_0)$$

where dC/dt is the slope of cumulative concentration in the receiver compartment *versus* time, V_r is the volume of the receiver compartment, V_d is the volume of the donor compartment, A is the membrane surface area, C_0 is the initial compound concentration in the donor chamber, C_r^{final} is the cumulative receiver concentration at the end of the incubation period, and C_d^{final} is the concentration of the donor at the end of the incubation period. The efflux ratio (ER) is defined as P_{app} (B-to-A)/ P_{app} (A-to-B).

Liver Microsomal Metabolic Stability Assay. For this assay, stock solutions of test compounds in DMSO (1 mM) were initially diluted to a concentration of 40.0 μM using 0.1 M potassium phosphate buffer (pH 7.4). Test compounds were then added to reaction wells at a final concentration of 1 μM , which was assumed to be well below K_m values to ensure linear reaction conditions (*i.e.*, avoid saturation). The final DMSO concentration was kept constant at 0.1%. Each compound was tested in duplicate for both time points (0 and 60 min). CD-1 mouse (male) or pooled human liver microsomes (Corning Gentest) were added to the reaction wells at a final concentration of 0.5 mg/mL (protein). The final volume for each reaction was 100 μL , which included the NADPH-regeneration solution (NRS) mix (Corning Gentest). This NRS mix comprised glucose 6-phosphate dehydrogenase, NADP⁺, MgCl₂, and glucose 6-phosphate. Reactions were carried out at 37 °C in an orbital shaker at 175 rpm. Upon completion of the 60 min time point, reactions were terminated by the addition of 2 V (200 μL) of ice-cold acetonitrile containing 0.5% formic acid and an internal standard. Samples were then centrifuged at 4000 rpm for 10 min to remove debris and precipitated proteins. Approximately 150 μL of supernatant was subsequently transferred to a new 96-well microplate for LC/MS analysis. Narrow-window mass extraction LC/MS analysis was performed for all samples using a Waters Acquity UPLC system with a Waters Xevo quadrupole-time-of-flight (Q-TOF) mass spectrometer to determine relative peak areas of the parent compounds. Chromatographic separations were performed on a Waters Acquity UPLC HSS T3 column (2.1 mm \times 100 mm, 100 Å, 1.8 μm , part no. 186003539) at 30 °C. Mobile phases A and B were 0.1% formic acid in water and 0.1% formic acid in acetonitrile, respectively. The sample temperature was kept at 10 °C. The typical injection volume was 0.3 μL . Chromatographic gradients used are shown in the table below.

Time (min)	Flow Rate ($\mu\text{L}/\text{min}$)	%A	%B
0.0	0.450	100	0
2.5	0.450	5	95
3.0	0.450	5	95
3.5	0.450	100	0
4.5	0.450	100	0

Data acquisition was performed in the electrospray (ES) positive ion mode in the mass range of 100–1000 m/z . The following source parameters were used: capillary voltage, 0.8 kV; cone voltage, 25 V; source temperature, 150 °C; desolvation temperature, 500 °C; cone gas flow, 150 L/h; desolvation gas flow, 600 L/h. Accurate masses were measured in the lock-spray automated exact mass measurement mode. The fragment ions of leucine-enkephalin were used as reference substances (lock-mass) in the acquisition mode. The following lock-spray configuration was used: frequency, 10 s; cone voltage, 25 V; collision energy, 22 V. Data processing was performed using MassLynx 4.1 software (Waters). The percentage remaining values were calculated using the following equation:

$$\text{percent remaining} = (A/A_0) \times 100$$

where A is area response after incubation and A_0 is area response at the initial time point.

Plasma Protein Binding Assay. A 48-well format rapid equilibrium dialysis (RED) device from Thermo Fisher Scientific was used for the plasma protein binding assay. Each RED device insert contained a buffer and a plasma compartment separated by a semipermeable membrane with a molecular weight cutoff of approximately 8 kDa. Stock solutions of test compounds in DMSO (1 mM) were spiked into heparinized pooled human plasma from Innovative Research (Novi, Michigan) at the final compound concentration of 5 μM (final DMSO concentration was 0.5%). The prepared plasma sample (300 μL) was added to a plasma chamber, and 500 μL of Dulbecco's phosphate-buffered saline (DPBS) was added to a buffer chamber. The RED plate was incubated in an orbital shaker at 37 °C and 200 rpm for 4 h. After the incubation, 50 μL aliquots of postdialysis samples from the buffer and the plasma chambers were transferred to a 96-well deep well plate. Samples were matrix-matched for the analysis by the addition of 50 μL of plasma to the buffer samples and 50 μL of buffer to the plasma samples. Ice-cold acetonitrile (300

μL) containing 0.5% formic acid and an internal standard was added to each well to precipitate plasma proteins. The deep well plate was tightly sealed with a plastic mat, mixed vigorously for 5 min, and placed on ice for 30 min. After the extraction step, the deep well plate was centrifuged for 10 min at 4000 rpm. Approximately 150 μL of supernatant was subsequently transferred to a new 96-well microplate for LC/MS analysis. Narrow-window mass extraction LC/MS analysis was performed for all samples using a Waters Acquity UPLC system with a Waters Xevo quadrupole-time-of-flight (Q-TOF) mass spectrometer to determine relative peak areas of the parent compounds. Chromatographic separations were performed on a Waters Acquity UPLC HSS T3 column (2.1 mm \times 100 mm, 100 Å, 1.8 μm , part no. 186003539) at 30 °C. Mobile phases A and B were 0.1% formic acid in water and 0.1% formic acid in acetonitrile, respectively. The sample temperature was kept at 10 °C. The typical injection volume was 0.3 μL . Chromatographic gradients used are shown in the table below.

Time (min)	Flow Rate ($\mu\text{L}/\text{min}$)	%A	%B
0.0	0.400	100	0
4.5	0.400	5	95
5.0	0.400	5	95
5.5	0.400	100	0
6.5	0.400	100	0

Data acquisition was performed in the electrospray (ES) positive ion mode in the mass range of 100–1000 m/z . The following source parameters were used: capillary voltage, 0.8 kV; cone voltage, 25 V; source temperature, 150 °C; desolvation temperature, 500 °C; cone gas flow, 150 L/h; desolvation gas flow, 600 L/h. Accurate masses were measured in the lock-spray automated exact mass measurement mode. The fragment ions of leucine-enkephalin were used as reference substances (lock-mass) in the acquisition mode. The following lock-spray configuration was used: frequency, 10 s; cone voltage, 25 V; collision energy, 22 V. Data processing was performed using MassLynx 4.1 software (Waters). Each determination was performed in triplicate. The percentage of the bound test compound was calculated using the following equation:

$$\text{percent bound} = 100 - [(A_{\text{buffer}}/A_{\text{plasma}}) \times 100]$$

where A_{buffer} is area response of the buffer chamber and A_{plasma} is area response of the plasma chamber.

hERG Potassium Channel Inhibition Assay. hERG IC₅₀ values were generated by Charles River Laboratories (Cleveland, Ohio). Compounds were tested against cloned hERG potassium channels expressed in HEK-293 cells. Chemicals used in solution preparation were purchased from Sigma-Aldrich (St. Louis, MO) unless otherwise noted and were of ACS reagent-grade purity or higher. Stock solutions of test articles and the positive control were prepared in dimethyl sulfoxide (DMSO) and stored frozen. Reference compound concentrations were prepared fresh daily by diluting stock solutions into a Charles River proprietary HEPES-buffered physiological saline (HB-PS) solution, which was prepared weekly and refrigerated until use. Because previous results have shown that $\leq 0.3\%$ DMSO did not affect channel currents, all test and control solutions contained 0.3% DMSO. Each test article formulation was sonicated (model 2510/5510, Branson Ultrasonics, Danbury, CT) at ambient room temperature for 20 min to facilitate dissolution. Cells were cultured in DMEM/nutrient mixture F-12 (D-MEM/F-12) supplemented with 10% FBS, 100 U/mL penicillin G sodium, 100 $\mu\text{g}/\text{mL}$ streptomycin sulfate, and 500 $\mu\text{g}/\text{mL}$ G418. Before testing, cells in culture dishes were washed twice with HBSS and detached with accutase. Immediately before use in the IonWorks Barracuda system, the cells were washed twice in HB-PS to remove the accutase and resuspended in 5 mL of HB-PS. The test article effects were evaluated using IonWorks Barracuda systems (Molecular Devices Corporation, Union City, CA). HEPES-buffered intracellular solution (Charles River proprietary) for whole-cell recordings was loaded into the intracellular compartment of the Population Patch Clamp (PPC) planar electrode. Extracellular buffer (HB-PS) was loaded into PPC planar electrode plate wells (11 μL per well). The cell suspension was pipetted into the wells of the PPC planar

electrode (9 μL per well). After establishment of a whole-cell configuration (the perforated patch), membrane currents were recorded using a patch clamp amplifier in the IonWorks Barracuda system. The current recordings were performed one time before test article application to the cells (baseline) and one time after application of the test article. Test article concentrations were applied to naive cells ($n = 4$, where $n =$ replicates per concentration). Each application consisted of addition of 20 μL of 2 \times concentrated test article solution to the total 40 μL of the final volume of the extracellular well of the PPC plate. The duration of exposure to each compound concentration was 5 min. The hERG current was measured using a pulse pattern with fixed amplitudes (conditioning prepulse: -80 mV for 25 ms; test pulse: $+40$ mV for 80 ms) from a holding potential of 0 mV ("zero holding" procedure). The hERG current was measured as a difference between the peak current at 1 ms after the test step to $+40$ mV and the steady-state current at the end of the step to $+40$ mV.

CYP Inhibition Assay. CYP IC_{50} values were generated by Pharmaron (Beijing, China). Multiple concentrations (1 μL) of the test compound or positive control compound (CYP1A2, furafylline; CYP2B6, ketoconazole; CYP2C8, quercetin; CYP2C9, sulfaphenazole; CYP2C19, *N*-3-benzylirivanol; CYP2D6, quinidine; and CYP3A4, ketoconazole) were transferred to the "compound plate". The concentrations of test compounds and positive control compounds were 0, 0.2, 1, 2, 10, 50, 200, 2000, and 10 000 μM . The master solution was prepared with MgCl_2 solution (20 μL of 50 mM solution), phosphate buffer (100 μL of 200 mM solution), ultrapure water (56 μL), human liver microsomes [2 μL of 20 mg/mL stock concentration (Corning 1328 UltraPool HLM 150, Mixed Gender, cat. no. 452117)], and 1 μL of substrate [CYP1A2, phenacetin (8 mM stock concentration); CYP2B6, bupropion (10 mM stock concentration); CYP2C8, paclitaxel (1 mM stock concentration); CYP2C9, tolbutamide (40 mM stock concentration); CYP2C19, mephenytoin (10 mM stock concentration); CYP2D6, dextromethorphan (2 mM stock concentration); and CYP3A4, midazolam (1 mM stock concentration), and testosterone (10 mM stock concentration)]. The master solution was prewarmed in a water bath at 37 $^{\circ}\text{C}$ for 5 min. The incubated master solution (179 μL) was transferred to the compound plate. In the mixed system, the final concentrations of the test compounds and positive control compounds were 0, 0.001, 0.005, 0.01, 0.05, 0.25, 1, 10, and 50 μM . All experiments were performed in duplicate. The reaction was started with the addition of 20 μL of 10 mM NADPH solution at the final concentration of 1 mM. The reaction was stopped by the addition of 1.5 V of methanol with IS (100 nM alprazolam, 200 nM imipramine, 200 nM labetalol, and 2 μM ketoprofen) to the "incubation plate" at the designated time points (20 min for CYP1A2, 2B6, 2C9, 2C19, and 2D6, 5 min for midazolam-mediated 3A4, and 10 min for testosterone-mediated 3A4). The incubation plate was centrifuged at 3220g for 40 min to precipitate the protein. An aliquot of 100 μL of the supernatant was diluted using 100 μL ultrapure water, and the mixture was used for LC/MS/MS analysis. The formation of metabolites was analyzed using LC/MS/MS. A decrease in the formation of the metabolites in the peak area to vehicle control was used to calculate the IC_{50} value (test compound concentration that produces 50% inhibition) using Excel Xlfit.

In Vivo Pharmacokinetic Studies. The pharmacokinetic profiles of 6a, 11b, 14g, 14k–l, and 14p were assessed by Pharmaron (Louisville, Kentucky), and all animal studies were performed in accordance with institutional guidelines as defined by the Institutional Animal Care and Use Committee. Test compounds were dissolved first in DMSO and then mixed with 47.5% PEG-400 and 47.5% deionized water with 10% Tween80. The solutions were thoroughly vortexed after each step and stored at room temperature. Solutions were freshly prepared on the day of dosing. Female CB17 SCID mice ($n = 3$) (6–8 weeks old, 17–20 g weight) were orally administered a 10 mg/kg dose (10 mL/kg dose volume, 1 mg/mL concentration) of the test compound. Blood samples were taken *via* the dorsal metatarsal vein at 0.25, 0.5, 1, 2, 4, 8, and 24 h postdosage. Blood samples were transferred into plastic microcentrifuge tubes containing the anticoagulant Heparin-Na and centrifuged at 4000g for 5 min at 4 $^{\circ}\text{C}$ to obtain

plasma. The samples were stored in a freezer at -75 ± 15 $^{\circ}\text{C}$ prior to analysis.

To determine brain concentrations, female CB17 SCID mice ($n = 3$) (6–8 weeks old, 17–20 g weight) were orally administered a 100 mg/kg dose (10 mL/kg dose volume, 10 mg/mL concentration) of the test compound. At 4 h postdose, the animals were terminally anesthetized by an increasing concentration of CO_2 . Their chest cavities were opened to expose the heart, and an incision at the right auricle using surgical scissors was done. A syringe full of gentle saline was pushed into the heart slowly *via* the left ventricle (saline volume ~ 10 mL). The animal was placed head down at a 45 $^{\circ}$ angle to facilitate blood removal. Brain samples were collected and kept frozen at -75 ± 15 $^{\circ}\text{C}$. All brain samples were weighed and homogenized with phosphate-buffered saline by a brain weight (g)-to-buffer volume (mL) ratio of 1:3 before analysis. The actual concentrations were the detected value multiplied using the dilution factor.

Concentrations of the test compound in the plasma samples were analyzed using an LC/MS/MS method. WinNonlin (Phoenix, version 8.0) or other similar software was used for pharmacokinetic calculations. The following pharmacokinetic parameters were calculated, whenever possible, from the plasma concentration *versus* time data following PO administration: $t_{1/2}$, C_{max} , T_{max} , AUC_{last} , AUC_{inf} , and F .

Cocrystallization of ALK2 with M4K2009. Protein Expression and Purification. Constructs were prepared by ligation-independent cloning. The kinase domain of ALK2 (residues 201–499; Uniprot ID, Q04771) was cloned into pFB-LIC-Bse for the baculoviral expression. The construct was verified by sequencing. ALK2 was expressed in Sf9 insect cells grown at 27 $^{\circ}\text{C}$. Some 72 h postinfection, cells were harvested and lysed using ultrasonication. ALK2 was initially purified by nickel affinity chromatography before subsequent purification by size exclusion chromatography (Superdex 200 16/600). The eluted protein was stored in 50 mM HEPES, pH 7.5, 300 mM NaCl, 10 mM DTT. The hexahistidine tag of ALK2 was cleaved using tobacco etch virus protease after initial nickel purification.

Crystallization. Crystallization was achieved at 4 $^{\circ}\text{C}$ using the sitting-drop vapor diffusion method. ALK2 was preincubated with 1 mM M4K2009 at a protein concentration of 11 mg/mL and crystallized using a precipitant containing 0.1 M citrate pH 4.9, 1 M ammonium sulfate, and 0.2 M sodium/potassium tartrate. Viable crystals were obtained when the protein solution was mixed with the reservoir solution at a 2:1 volume ratio. Crystals were cryoprotected with mother liquor plus 25% ethylene glycol prior to vitrification in liquid nitrogen.

Data Collection. Diffraction data were collected at the Diamond Light Source, station I03 using monochromatic radiation at a wavelength of 0.9686 \AA .

Phasing, Model Building, Refinement, and Validation. Data were processed with Xia2 and subsequently scaled using the program AIMLESS from the CCP4 suite.^{64,65} Initial phases were obtained by molecular replacement using the program PHASER and the structure of ALK2 (Protein Data Bank code 6SZM) as a search model.⁶⁶ The resulting structure solution was refined using Phenix Refine and manually rebuilt with COOT.^{67,68} The complete structure was verified for geometric correctness with MolProbity.⁶⁹ Data collection and refinement statistics can be found in the Supporting Information, Table S3. Cocrystal images in the article were processed using Molsoft MolBrowser 3.8, and the 2D ligand interaction plot was generated using Maestro (Schrodinger Release 2019-4, Schrodinger, LLC, New York).

■ ASSOCIATED CONTENT

Supporting Information

The Supporting Information is available free of charge at <https://pubs.acs.org/doi/10.1021/acs.jmedchem.0c01199>.

Kinase selectivity panel, safety screen panel, ALK2-M4K2009 cocrystal data collection and refinement statistics, ^1H spectra and HPLC traces of select compounds (PDF)

Molecular formula strings (CSV)

Accession Codes

PBD ID codes: ALK2-M4K2009, 6SZM; ALK2-LDN-213844, 4BGG.

AUTHOR INFORMATION**Corresponding Authors**

David Smil – Drug Discovery Program, Ontario Institute for Cancer Research, 661 University Avenue, Toronto, Ontario M5G 0A3, Canada; orcid.org/0000-0002-6232-6087; Phone: +1 (647) 260-6454; Email: david.smil@oicr.on.ca

Methvin B. Isaac – Drug Discovery Program, Ontario Institute for Cancer Research, 661 University Avenue, Toronto, Ontario M5G 0A3, Canada; Phone: +1 (416) 673-6655; Email: methvin.isaac@oicr.on.ca

Authors

Jong Fu Wong – Structural Genomics Consortium, University of Oxford, Oxford OX3 7DQ, United Kingdom

Eleanor P. Williams – Structural Genomics Consortium, University of Oxford, Oxford OX3 7DQ, United Kingdom

Roslin J. Adamson – Structural Genomics Consortium, University of Oxford, Oxford OX3 7DQ, United Kingdom

Alison Howarth – Structural Genomics Consortium, University of Oxford, Oxford OX3 7DQ, United Kingdom

David A. McLeod – Drug Discovery Program, Ontario Institute for Cancer Research, 661 University Avenue, Toronto, Ontario M5G 0A3, Canada

Ahmed Mamai – Drug Discovery Program, Ontario Institute for Cancer Research, 661 University Avenue, Toronto, Ontario M5G 0A3, Canada

Soyoung Kim – Drug Discovery Program, Ontario Institute for Cancer Research, 661 University Avenue, Toronto, Ontario M5G 0A3, Canada

Brian J. Wilson – Drug Discovery Program, Ontario Institute for Cancer Research, 661 University Avenue, Toronto, Ontario M5G 0A3, Canada

Taira Kiyota – Drug Discovery Program, Ontario Institute for Cancer Research, 661 University Avenue, Toronto, Ontario M5G 0A3, Canada

Ahmed Aman – Drug Discovery Program, Ontario Institute for Cancer Research, 661 University Avenue, Toronto, Ontario M5G 0A3, Canada; Leslie Dan Faculty of Pharmacy, University of Toronto, Toronto, Ontario M5S 3M2, Canada

Julie Owen – Drug Discovery Program, Ontario Institute for Cancer Research, 661 University Avenue, Toronto, Ontario M5G 0A3, Canada

Gennady Poda – Drug Discovery Program, Ontario Institute for Cancer Research, 661 University Avenue, Toronto, Ontario M5G 0A3, Canada; Leslie Dan Faculty of Pharmacy, University of Toronto, Toronto, Ontario M5S 3M2, Canada

Kurumi Y. Horiuchi – Reaction Biology Corp., Malvern, Pennsylvania 19355, United States

Ekaterina Kuznetsova – Reaction Biology Corp., Malvern, Pennsylvania 19355, United States

Haiching Ma – Reaction Biology Corp., Malvern, Pennsylvania 19355, United States

J. Nicole Hamblin – Charles River Discovery, Essex CB10 1XL, United Kingdom

Sue Cramp – Charles River Discovery, Essex CM19 5TR, United Kingdom

Owen G. Roberts – M4K Pharma, Toronto, Ontario M5G 1L7, Canada

Aled M. Edwards – M4K Pharma, Toronto, Ontario M5G 1L7, Canada; Structural Genomics Consortium, University of Toronto, Toronto, Ontario M5G 1L7, Canada; orcid.org/0000-0002-4782-6016

David Uehling – Drug Discovery Program, Ontario Institute for Cancer Research, 661 University Avenue, Toronto, Ontario M5G 0A3, Canada

Rima Al-awar – Drug Discovery Program, Ontario Institute for Cancer Research, 661 University Avenue, Toronto, Ontario M5G 0A3, Canada; Department of Pharmacology and Toxicology, University of Toronto, Toronto, Ontario M5S 1A8, Canada; orcid.org/0000-0002-4185-055X

Alex N. Bullock – Structural Genomics Consortium, University of Oxford, Oxford OX3 7DQ, United Kingdom; orcid.org/0000-0001-6757-0436

Jeff A. O'Meara – Drug Discovery Program, Ontario Institute for Cancer Research, 661 University Avenue, Toronto, Ontario M5G 0A3, Canada; M4K Pharma, Toronto, Ontario M5G 1L7, Canada

Complete contact information is available at:

<https://pubs.acs.org/10.1021/acs.jmedchem.0c01199>

Author Contributions

Compounds were designed and their syntheses were devised by D.S., D.A.M., and B.J.W. Compounds were synthesized by D.S., D.A.M., and S.K. *In vitro* kinase screening data was generated by K.Y.H., E.K., and H.M. NanoBRET and DLA data were generated by J.F.W. and A.H. Crystallography experiments were performed by E.P.W. and R.J.A. Caco-2, microsomal stability, and PPB studies were conducted by T.K. HRMS data were generated by T.K. J.O. created the cocrystal structure graphics. G.P. generated the Oracle database where compound data were stored. A.M., A.A., J.N.H., S.C., D.U., R.A.-a., A.N.B., J.A.O., and M.B.I. were involved in experimental design, interpretation of data, and monitored project progress. O.G.R. and A.M.E. initiated the project, monitored project progress, and edited the paper. The manuscript was written by D.S. and revised by A.M.E., R.A.-a., A.N.B., and M.B.I.

Notes

The authors declare no competing financial interest.

The authors will release the atomic coordinates and experimental data upon article publication.

ACKNOWLEDGMENTS

M4K Pharma Inc., functioning as a virtual biotech, serves as a *de facto* hub for gathering and aligning the cooperation and contributions of academic and industry partners into a drug development program that operates free of restrictions on data disclosure (*i.e.*, no patents are filed). Work was performed by nonprofit organizations, the Ontario Institute for Cancer Research (OICR), and the Structural Genomics Consortium (SGC), with additional biological evaluation of compounds made possible through the in-kind contributions of collaborators at Reaction Biology Corporation and Charles River Laboratories. This work was funded by the Cancer Therapeutics Innovation Pipeline program at the OICR, which receives financial support from the Government of Ontario through the Ministry of Training, Colleges, and Universities. Funding from The Brain Tumour Charity was used to support the cellular and crystallographic research conducted at the University of Oxford. The SGC is a registered charity (number 1097737) that receives funds from AbbVie, Bayer Pharma AG, Boehringer Ingelheim,

Canada Foundation for Innovation, Eshelman Institute for Innovation, Genome Canada through the Ontario Genomics Institute [OGI-055], Innovative Medicines Initiative (EU/EFPIA) [ULTRA-DD grant no. 115766], Janssen, Merck KGaA, Darmstadt, Germany, MSD, Novartis Pharma AG, Pfizer, Sao Paulo Research Foundation-FAPESP, Takeda, and Wellcome [106169/ZZ14/Z]. The authors thank the Reaction Biology Corporation kinase assay group for their *pro bono* contribution to the *in vitro* kinase screening and Charles River Laboratories Cleveland for all hERG activity screening. The authors also thank Mehakpreet Saini for contributing to the writing and editing of ADME protocols.

ABBREVIATIONS

ALK2, activin receptor-like kinase-2; BMP, bone morphogenetic protein; B/P, total brain-to-plasma ratio; BRET, bioluminescence resonance energy transfer; BTB, brain tissue binding; C_{max} , maximum concentration; DIPG, diffuse intrinsic pontine glioma; DLA, dual luciferase assay; EDG, electron donating group; EWG, electron withdrawing group; FOP, fibrodysplasia ossificans progressiva; GS, glycine-serine; HLM, human liver microsome; MLM, mouse liver microsome; TGF β , transforming growth factor β

REFERENCES

- (1) Girardi, F.; Allemani, C.; Coleman, M. P. Worldwide trends in survival from common childhood brain tumors: a systematic review. *J. Global Oncol.* **2019**, *5*, 1–25.
- (2) Pacifici, M.; Shore, E. M. Common mutations in ALK2/ACVR1, a multi-faceted receptor, have roles in distinct pediatric musculoskeletal and neural orphan disorders. *Cytokine Growth Factor Rev.* **2016**, *27*, 93–104.
- (3) Taylor, K. R.; Mackay, A.; Truffaux, N.; Butterfield, Y. S.; Morozova, O.; Philippe, C.; Castel, D.; Grasso, C. S.; Vinci, M.; Carvalho, D.; Carcaboso, A. M.; de Torres, C.; Cruz, O.; Mora, J.; Entz-Werle, N.; Ingram, W. J.; Monje, M.; Hargrave, D.; Bullock, A. N.; Puget, S.; Yip, S.; Jones, C.; Grill, J. Recurrent activating ACVR1 mutations in diffuse intrinsic pontine glioma. *Nat. Genet.* **2014**, *46*, 457–461.
- (4) Mathew, R. K.; Rutka, J. T. Diffuse intrinsic pontine glioma: clinical features, molecular genetics, and novel targeted therapeutics. *J. Korean Neurosurg. Soc.* **2018**, *61*, 343–351.
- (5) Hoffman, L. M.; Veldhuijzen van Zanten, S. E. M.; Colditz, N.; Baugh, J.; Chaney, B.; Hoffmann, M.; Lane, A.; Fuller, C.; Miles, L.; Hawkins, C.; Bartels, U.; Bouffet, E.; Goldman, S.; Leary, S.; Foreman, N. K.; Packer, R.; Warren, K. E.; Broniscer, A.; Kieran, M. W.; Minturn, J.; Comito, M.; Broxson, E.; Shih, C. S.; Khatua, S.; Chintagumpala, M.; Carret, A. S.; Escorza, N. Y.; Hassall, T.; Ziegler, D. S.; Gottardo, N.; Dholaria, H.; Doughman, R.; Benesch, M.; Drissi, R.; Nazarian, J.; Jabado, N.; Boddaert, N.; Varlet, P.; Giraud, G.; Castel, D.; Puget, S.; Jones, C.; Hulleman, E.; Modena, P.; Giagnacovo, M.; Antonelli, M.; Pietsch, T.; Gielen, G. H.; Jones, D. T. W.; Sturm, D.; Pfister, S. M.; Gerber, N. U.; Grotzer, M. A.; Pfaff, E.; von Bueren, A. O.; Hargrave, D.; Solanki, G. A.; Jadrijevic Bivrlje, F.; Kaspers, G. J. L.; Vandertop, W. P.; Grill, J.; Bailey, S.; Biondi, V.; Massimino, M.; Calmon, R.; Sanchez, E.; Bison, B.; Warmuth-Metz, M.; Leach, J.; Jones, B.; van Vuurden, D. G.; Kramm, C. M.; Fouladi, M. Clinical, radiologic, pathologic, and molecular characteristics of long-term survivors of diffuse intrinsic pontine glioma (DIPG): a collaborative report from the international and european society for pediatric oncology DIPG registries. *J. Clin. Oncol.* **2018**, *36*, 1963–1972.
- (6) Warren, K. E. Diffuse intrinsic pontine glioma: poised for progress. *Front. Oncol.* **2012**, *2*, 205.
- (7) Janssens, G. O.; Gandola, L.; Bolle, S.; Mandeville, H.; Ramos-Albiac, M.; van Beek, K.; Benghiat, H.; Hoeben, B.; Morales La Madrid, A.; Kortmann, R. D.; Hargrave, D.; Menten, J.; Pecori, E.; Biondi, V.;

von Bueren, A. O.; van Vuurden, D. G.; Massimino, M.; Sturm, D.; Peters, M.; Kramm, C. M. Survival benefit for patients with diffuse intrinsic pontine glioma (DIPG) undergoing re-irradiation at first progression: a matched-cohort analysis on behalf of the SIOP-E-HGG/DIPG working group. *Eur. J. Cancer* **2017**, *73*, 38–47.

- (8) Di, L.; Rong, H.; Feng, B. Demystifying brain penetration in central nervous system drug discovery. *J. Med. Chem.* **2013**, *56*, 2–12.

- (9) Cohen, K. J.; Heideman, R. L.; Zhou, T.; Holmes, E. J.; Lavey, R. S.; Bouffet, E.; Pollack, I. F. Temozolomide in the treatment of children with newly diagnosed diffuse intrinsic pontine gliomas: a report from the Children's Oncology Group. *Neuro-Oncol.* **2011**, *13*, 410–416.

- (10) Korones, D. N.; Fisher, P. G.; Kretschmar, C.; Zhou, T.; Chen, Z.; Kepner, J.; Freeman, C. Treatment of children with diffuse intrinsic brain stem glioma with radiotherapy, vincristine and oral VP-16: a children's oncology group phase II study. *Pediatr. Blood Cancer* **2008**, *50*, 227–230.

- (11) Roujeau, T.; Machado, G.; Garnett, M. R.; Miquel, C.; Puget, S.; Georger, B.; Grill, J.; Boddaert, N.; Di Rocco, F.; Zerah, M.; Sainte-Rose, C. Stereotactic biopsy of diffuse pontine lesions in children. *J. Neurosurg.* **2007**, *107*, 1–4.

- (12) Jones, C.; Karajannis, M. A.; Jones, D. T. W.; Kieran, M. W.; Monje, M.; Baker, S. J.; Becher, O. J.; Cho, Y. J.; Gupta, N.; Hawkins, C.; Hargrave, D.; Haas-Kogan, D. A.; Jabado, N.; Li, X. N.; Mueller, S.; Nicolaides, T.; Packer, R. J.; Persson, A. I.; Phillips, J. J.; Simonds, E. F.; Stafford, J. M.; Tang, Y.; Pfister, S. M.; Weiss, W. A. Pediatric high-grade glioma: biologically and clinically in need of new thinking. *Neuro-Oncol.* **2017**, *19*, 153–161.

- (13) Mackay, A.; Burford, A.; Carvalho, D.; Izquierdo, E.; Fazal-Salom, J.; Taylor, K. R.; Bjerke, L.; Clarke, M.; Vinci, M.; Nandhabalan, M.; Temelso, S.; Popov, S.; Molinari, V.; Raman, P.; Waanders, A. J.; Han, H. J.; Gupta, S.; Marshall, L.; Zacharoulis, S.; Vaidya, S.; Mandeville, H. C.; Bridges, L. R.; Martin, A. J.; Al-Sarraj, S.; Chandler, C.; Ng, H. K.; Li, X.; Mu, K.; Trabelsi, S.; Brahim, D. H.; Kisljakov, A. N.; Konovalov, D. M.; Moore, A. S.; Carcaboso, A. M.; Sunol, M.; de Torres, C.; Cruz, O.; Mora, J.; Shats, L. I.; Stavale, J. N.; Bidinotto, L. T.; Reis, R. M.; Entz-Werle, N.; Farrell, M.; Cryan, J.; Crimmins, D.; Caird, J.; Pears, J.; Monje, M.; Debily, M. A.; Castel, D.; Grill, J.; Hawkins, C.; Nikbakht, H.; Jabado, N.; Baker, S. J.; Pfister, S. M.; Jones, D. T. W.; Fouladi, M.; von Bueren, A. O.; Baudis, M.; Sernick, A.; Jones, C. Integrated molecular meta-analysis of 1,000 pediatric high-grade and diffuse intrinsic pontine glioma. *Cancer Cell* **2017**, *32*, S20–S37.

- (14) Jones, C.; Baker, S. J. Unique genetic and epigenetic mechanisms driving paediatric diffuse high-grade glioma. *Nat. Rev. Cancer* **2014**, *14*, 651–661.

- (15) Mele, M.; Ferreira, P. G.; Reverter, F.; DeLuca, D. S.; Monlong, J.; Sammeth, M.; Young, T. R.; Goldmann, J. M.; Pervouchine, D. D.; Sullivan, T. J.; Johnson, R.; Segre, A. V.; Djebali, S.; Niarchou, A.; The GTEx Consortium; Wright, F. A.; Lappalainen, T.; Calvo, M.; Getz, G.; Dermizakis, E. T.; Ardlie, K. G.; Guigo, R. The human transcriptome across tissues and individuals. *Science* **2015**, *348*, 660–665.

- (16) Taylor, K. R.; Vinci, M.; Bullock, A. N.; Jones, C. ACVR1 mutations in DIPG: lessons learned from FOP. *Cancer Res.* **2014**, *74*, 4565–4570.

- (17) Shore, E. M.; Xu, M.; Feldman, G. J.; Fenstermacher, D. A.; Cho, T. J.; Choi, I. H.; Connor, J. M.; Delai, P.; Glaser, D. L.; LeMerrer, M.; Morhart, R.; Rogers, J. G.; Smith, R.; Triffitt, J. T.; Urtizberea, J. A.; Zasloff, M.; Brown, M. A.; Kaplan, F. S. A recurrent mutation in the BMP type I receptor ACVR1 causes inherited and sporadic fibrodysplasia ossificans progressiva. *Nat. Genet.* **2006**, *38*, 525–527.

- (18) Kaplan, F. S.; Xu, M.; Seemann, P.; Connor, J. M.; Glaser, D. L.; Carroll, L.; Delai, P.; Fastnacht-Urban, E.; Forman, S. J.; Gillissen-Kaesbach, G.; Hoover-Fong, J.; Koster, B.; Pauli, R. M.; Reardon, W.; Zaidi, S. A.; Zasloff, M.; Morhart, R.; Mundlos, S.; Groppe, J.; Shore, E. M. Classic and atypical fibrodysplasia ossificans progressiva (FOP) phenotypes are caused by mutations in the bone morphogenetic protein (BMP) type I receptor ACVR1. *Hum. Mutat.* **2009**, *30*, 379–390.

- (19) Nikbakht, H.; Panditharatna, E.; Mikael, L. G.; Li, R.; Gayden, T.; Osmond, M.; Ho, C. Y.; Kambhampati, M.; Hwang, E. I.; Faury, D.; Siu,

- A.; Papillon-Cavanagh, S.; Bechet, D.; Ligon, K. L.; Ellezam, B.; Ingram, W. J.; Stinson, C.; Moore, A. S.; Warren, K. E.; Karamchandani, J.; Packer, R. J.; Jabado, N.; Majewski, J.; Nazarian, J. Spatial and temporal homogeneity of driver mutations in diffuse intrinsic pontine glioma. *Nat. Commun.* **2016**, *7*, No. 11185.
- (20) ten Dijke, P.; Ichijo, H.; Franzen, P.; Schulz, P.; Saras, J.; Toyoshima, H.; Heldin, C. H.; Miyazono, K. Activin receptor-like kinases: a novel subclass of cell-surface receptors with predicted serine/threonine kinase activity. *Oncogene* **1993**, *8*, 2879–2887.
- (21) Macias-Silva, M.; Hoodless, P. A.; Tang, S. J.; Buchwald, M.; Wrana, J. L. Specific activation of Smad1 signaling pathways by the BMP7 type I receptor, ALK2. *J. Biol. Chem.* **1998**, *273*, 25628–25636.
- (22) Lopez-Rovira, T.; Chalaux, E.; Massague, J.; Rosa, J. L.; Ventura, F. Direct binding of Smad1 and Smad4 to two distinct motifs mediates bone morphogenetic protein-specific transcriptional activation of Id1 gene. *J. Biol. Chem.* **2002**, *277*, 3176–3185.
- (23) Korchynski, O.; ten Dijke, P. Identification and functional characterization of distinct critically important bone morphogenetic protein-specific response elements in the Id1 promoter. *J. Biol. Chem.* **2002**, *277*, 4883–4891.
- (24) Hino, K.; Ikeya, M.; Horigome, K.; Matsumoto, Y.; Ebise, H.; Nishio, M.; Sekiguchi, K.; Shibata, M.; Nagata, S.; Matsuda, S.; Toguchida, J. Neofunction of ACVR1 in fibrodysplasia ossificans progressiva. *Proc. Natl. Acad. Sci. U.S.A.* **2015**, *112*, 15438–15443.
- (25) Hatsell, S. J.; Idone, V.; Wolken, D. M.; Huang, L.; Kim, H. J.; Wang, L.; Wen, X.; Nannuru, K. C.; Jimenez, J.; Xie, L.; Das, N.; Makhoul, G.; Chernomorsky, R.; D'Ambrosio, D.; Corpina, R. A.; Schoenherr, C. J.; Feeley, K.; Yu, P. B.; Yancopoulos, G. D.; Murphy, A. J.; Economides, A. N. ACVR1R206H receptor mutation causes fibrodysplasia ossificans progressiva by imparting responsiveness to activin A. *Sci. Transl. Med.* **2015**, *7*, No. 303ra137.
- (26) Wu, G.; Diaz, A. K.; Pugh, B. S.; Rankin, S. L.; Ju, B.; Li, Y.; Zhu, X.; Qu, C.; Chen, X.; Zhang, J.; Easton, J.; Edmonson, M.; Ma, X.; Lu, C.; Nagahawatte, P.; Hedlund, E.; Rusch, M.; Pounds, S.; Lin, T.; Onar-Thomas, A.; Huether, R.; Kriwacki, R.; Parker, M.; Gupta, P.; Becksfors, J.; Wei, L.; Mulder, H. L.; Boggs, K.; Vadodaria, B.; Yergeau, D.; Russell, J. C.; Ochoa, K.; Fulton, R. S.; Fulton, L. L.; Jones, C.; Boop, F. A.; Broniscer, A.; Wetmore, C.; Gajjar, A.; Ding, L.; Mardis, E. R.; Wilson, R. K.; Taylor, M. R.; Downing, J. R.; Ellison, D. W.; Zhang, J.; Baker, S. J. The genomic landscape of diffuse intrinsic pontine glioma and pediatric non-brainstem high-grade glioma. *Nat. Genet.* **2014**, *46*, 444–450.
- (27) Hoeman, C. M.; Cordero, F. J.; Hu, G.; Misuraca, K.; Romero, M. M.; Cardona, H. J.; Nazarian, J.; Hashizume, R.; McLendon, R.; Yu, P.; Procissi, D.; Gadd, S.; Becher, O. J. ACVR1 R206H cooperates with H3.1K27M in promoting diffuse intrinsic pontine glioma pathogenesis. *Nat. Commun.* **2019**, *10*, No. 1023.
- (28) Yu, P. B.; Hong, C. C.; Sachidanandan, C.; Babitt, J. L.; Deng, D. Y.; Hoyng, S. A.; Lin, H. Y.; Bloch, K. D.; Peterson, R. T. Dorsomorphin inhibits BMP signals required for embryogenesis and iron metabolism. *Nat. Chem. Biol.* **2008**, *4*, 33–41.
- (29) Hopkins, C. R. Inhibitors of the bone morphogenetic protein (BMP) signaling pathway: a patent review (2008-2015). *Expert Opin. Ther. Pat.* **2016**, *26*, 1115–1128.
- (30) Cuny, G. D.; Yu, P. B.; Laha, J. K.; Xing, X.; Liu, J.-F.; Lai, C. S.; Deng, D. Y.; Sachidanandan, C.; Bloch, K. D.; Peterson, R. T. Structure-activity relationship study of bone morphogenetic protein (BMP) signaling inhibitors. *Bioorg. Med. Chem. Lett.* **2008**, *18*, 4388–4392.
- (31) Mohedas, A. H.; Xing, X.; Armstrong, K. A.; Bullock, A. N.; Cuny, G. D.; Yu, P. B. Development of an ALK2-biased BMP type I receptor kinase inhibitor. *ACS Chem. Biol.* **2013**, *8*, 1291–1302.
- (32) Williams, E.; Bullock, A. N. Structural basis for the potent and selective binding of LDN-212854 to the BMP receptor kinase ALK2. *Bone* **2018**, *109*, 251–258.
- (33) Yu, P. B.; Deng, D. Y.; Lai, C. S.; Hong, C. C.; Cuny, G. D.; Bouxsein, M. L.; Hong, D. W.; McManus, P. M.; Katagiri, T.; Sachidanandan, C.; Kamiya, N.; Fukuda, T.; Mishina, Y.; Peterson, R. T.; Bloch, K. D. BMP type I receptor inhibition reduces heterotopic [corrected] ossification. *Nat. Med.* **2008**, *14*, 1363–1369.
- (34) Vogt, J.; Traynor, R.; Sapkota, G. P. The specificities of small molecule inhibitors of the TGF β and BMP pathways. *Cell. Signalling* **2011**, *23*, 1831–1842.
- (35) Sinha, S.; Mundy, C.; Bechtold, T.; Sgariglia, F.; Ibrahim, M. M.; Billings, P. C.; Carroll, K.; Koyama, E.; Jones, K. B.; Pacific, M. Unsuspected osteochondroma-like outgrowths in the crania base of hereditary multiple exostoses patients and modeling and treatment with a BMP antagonist in mice. *PLoS Genet.* **2017**, *13*, No. e1006742.
- (36) Sanvitale, C. E.; Kerr, G.; Chaikuad, A.; Ramel, M. C.; Mohedas, A. H.; Reichert, S.; Wang, Y.; Triffitt, J. T.; Cuny, G. D.; Yu, P. B.; Hill, C. S.; Bullock, A. N. A new class of small molecule inhibitor of BMP signaling. *PLoS One* **2013**, *8*, No. e62721.
- (37) Mohedas, A. H.; Wang, Y.; Sanvitale, C. E.; Canning, P.; Choi, S.; Xing, X.; Bullock, A. N.; Cuny, G. D.; Yu, P. B. Structure-activity relationship of 3,5-diaryl-2-aminopyridine ALK2 inhibitors reveals unaltered binding affinity for fibrodysplasia ossificans progressiva causing mutants. *J. Med. Chem.* **2014**, *57*, 7900–7915.
- (38) Jiang, J.-k.; Huang, X.; Shamim, K.; Patel, P. R.; Lee, A.; Wang, A. Q.; Nguyen, K.; Tawa, G.; Cuny, G. D.; Yu, P. B.; Zheng, W.; Xu, X.; Sanderson, P.; Huang, W. Discovery of 3-(4-sulfamoylnaphthyl)pyrazolo[1,5-a]pyrimidines as potent and selective ALK2 inhibitors. *Bioorg. Med. Chem. Lett.* **2018**, *28*, 3356–3362.
- (39) Hudson, L.; Mui, J.; Vazquez, S.; Carvalho, D. M.; Williams, E.; Jones, C.; Bullock, A. N.; Hoelder, S. Novel quinazolinone inhibitors of ALK2 flip between alternate binding modes: structure-activity relationship, structural characterization, kinase profiling, and cellular proof of concept. *J. Med. Chem.* **2018**, *61*, 7261–7272.
- (40) Sekimata, K.; Sato, T.; Sakai, N.; Watanabe, H.; Mishima-Tsumagari, C.; Taguri, T.; Matsumoto, T.; Fujii, Y.; Handa, N.; Honma, T.; Tanaka, A.; Shirouzu, M.; Yokoyama, S.; Miyazono, K.; Hashizume, Y.; Koyama, H. Bis-heteroaryl pyrazoles: identification of orally bioavailable inhibitors of activin receptor-like kinase-2 (R206H). *Chem. Pharm. Bull. (Tokyo)* **2019**, *67*, 224–235.
- (41) Sanchez-Duffhues, G.; Williams, E.; Benderitter, P.; Orlova, V.; van Wijhe, M.; Garcia de Vinuesa, A.; Kerr, G.; Caradec, J.; Lodder, K.; de Boer, H. C.; Goumans, M.-J.; Eekhoff, E. M. W.; Morales-Piga, A.; Bachiller-Corral, J.; Koolwijk, P.; Bullock, A. N.; Hoflack, J.; ten Dijke, P. Development of macrocycle kinase inhibitors for ALK2 using fibrodysplasia ossificans progressiva-derived endothelial cells. *JBM R Plus* **2019**, *3*, No. e10230.
- (42) Wentworth, K. L.; Masharani, U.; Hsiao, E. C. Therapeutic advances for blocking heterotopic ossification in fibrodysplasia ossificans progressiva. *Br. J. Clin. Pharmacol.* **2019**, *85*, 1180–1187.
- (43) Carvalho, D.; Taylor, K. R.; Olaciregui, N. G.; Molinari, V.; Clarke, M.; Mackay, A.; Ruddle, R.; Henley, A.; Valenti, M.; Hayes, A.; Brandon, A. H.; Eccles, S. A.; Raynaud, F.; Boudhar, A.; Monje, M.; Popov, S.; Moore, A. S.; Mora, J.; Cruz, O.; Vinci, M.; Brennan, P. E.; Bullock, A. N.; Carcaboso, A. M.; Jones, C. ALK2 inhibitors display beneficial effects in preclinical models of ACVR1 mutant diffuse intrinsic pontine glioma. *Commun. Biol.* **2019**, *2*, No. 156.
- (44) Morgan, M. R.; Roberts, O. G.; Edwards, A. M. Ideation and implementation of an open science drug discovery business model - M4K Pharma. *Wellcome Open Res.* **2018**, *3*, 154.
- (45) Wong, J. F.; Brown, E. J.; Williams, E.; Bullock, A. N. Fostering open collaboration in drug development for paediatric brain tumours. *Biochem. Soc. Trans.* **2019**, *47*, 1471–1479.
- (46) Herbertz, S.; Sawyer, J. S.; Stauber, A. J.; Gueorguieva, I.; Driscoll, K. E.; Estrem, S. T.; Cleverly, A. L.; Desai, D.; Guba, S. C.; Benhadji, K. A.; Slapak, C. A.; Lahn, M. M. Clinical development of galunisertib (LY2157299 monohydrate), a small molecule inhibitor of transforming growth factor-beta signaling pathway. *Drug Des., Dev. Ther.* **2015**, *9*, 4479–4499.
- (47) Pasteuning-Vuhman, S.; Boertje-van der Meulen, J. W.; van Putten, M.; Overzier, M.; ten Dijke, P.; Kielbasa, S. M.; Arindrarto, W.; Wolterbeek, R.; Lezhnina, K. V.; Ozerov, I. V.; Aliper, A. M.; Hoogaars, W. M.; Aartsma-Rus, A.; Loomans, C. J. M. New function of the myostatin/activin type I receptor (ALK4) as a mediator of muscle atrophy and muscle regeneration. *FASEB J.* **2017**, *31*, 238–255.

- (48) Roman, B. L.; Hinck, A. P. ALK1 signaling in development and disease: new paradigms. *Cell. Mol. Life Sci.* **2017**, *74*, 4539–4560.
- (49) Steinbicker, A. U.; Bartnikas, T. B.; Lohmeyer, L. K.; Leyton, P.; Mayeur, C.; Kao, S. M.; Pappas, A. E.; Peterson, R. T.; Bloch, D. B.; Yu, P. B.; Fleming, M. D.; Bloch, K. D. Perturbation of hepcidin expression by BMP type I receptor deletion induces iron overload in mice. *Blood* **2011**, *118*, 4224–4230.
- (50) Goff, L. W.; Cohen, R. B.; Berlin, J. D.; de Braud, F. G.; Lyschik, A.; Noberasco, C.; Bertolini, F.; Carpentieri, M.; Stampino, C. G.; Abbattista, A.; Wang, E.; Borghaei, H. A Phase I study of the anti-activin receptor-like kinase 1 (ALK-1) monoclonal antibody PF-03446962 in patients with advanced solid tumors. *Clin. Cancer Res.* **2016**, *22*, 2146–2154.
- (51) Pajouhesh, H.; Lenz, G. R. Medicinal chemistry properties of successful central nervous system drugs. *NeuroRx* **2005**, *2*, 541–553.
- (52) Rankovic, Z. CNS drug design: balancing physicochemical properties for optimal brain exposure. *J. Med. Chem.* **2015**, *58*, 2584–2608.
- (53) Heffron, T. P. Small molecule kinase inhibitors for the treatment of brain cancer. *J. Med. Chem.* **2016**, *59*, 10030–10066.
- (54) Sanguinetti, M. C.; Tristani-Firouzi, M. hERG potassium channels and cardiac arrhythmia. *Nature* **2006**, *440*, 463–469.
- (55) Shah, R. R.; Morganroth, J.; Shah, D. R. Cardiovascular safety of tyrosine kinase inhibitors: with a special focus on cardiac repolarisation (QT interval). *Drug Saf.* **2013**, *36*, 295–316.
- (56) Smil, D.; McLeod, D. A.; O'Meara, J. A.; Isaac, M. B. Unpublished results. Data can be viewed in presentations archived at <https://m4kpharma.com/blog/> (accessed Jul 10, 2020).
- (57) Ensan, D.; Smil, D.; Zepeda-Velazquez, C. A.; Panagopoulos, D.; Wong, J. F.; Williams, E. P.; Adamson, R.; Bullock, A. N.; Kiyota, T.; Aman, A.; Roberts, O. G.; Edwards, A. M.; O'Meara, J. A.; Isaac, M. B.; Al-awar, R. Targeting ALK2: an open science approach to developing therapeutics for the treatment of diffuse intrinsic pontine glioma. *J. Med. Chem.* **2020**, *63*, 4978–4996.
- (58) Predicted cLogP, pKa, and tPSA values were calculated using ChemDraw Professional 17.1.
- (59) Cavalli, A.; Poluzzi, E.; De Ponti, F.; Recanatini, M. Toward a pharmacophore for drugs inducing the long QT syndrome: insights from a CoMFA study of HERG K⁺ channel blockers. *J. Med. Chem.* **2002**, *45*, 3844–3853.
- (60) Jamieson, C.; Moir, E. M.; Rankovic, Z.; Wishart, G. Medicinal chemistry of hERG optimizations: highlights and hang-ups. *J. Med. Chem.* **2006**, *49*, 5029–5046.
- (61) Morgenthaler, M.; Schweizer, E.; Hoffmann-Roder, A.; Benini, F.; Martin, R. E.; Jaeschke, G.; Wagner, B.; Fischer, H.; Bendels, S.; Zimmerli, D.; Schneider, J.; Diederich, F.; Kansy, M.; Muller, K. Predicting and tuning physicochemical properties in lead optimization: amine basicities. *ChemMedChem* **2007**, *2*, 1100–1115.
- (62) Liu, X.; Wright, M.; Hop, C. E. C. A. Rational use of plasma protein and tissue binding data in drug design. *J. Med. Chem.* **2014**, *57*, 8238–8248.
- (63) Chakkalakal, S. A.; Shore, E. M. Heterotopic Ossification in Mouse Models of Fibrodysplasia Ossificans Progressiva. In *Bone Morphogenetic Proteins: Methods and Protocols (Methods in Molecular Biology)*; Rogers, M. B., Ed.; Springer Nature: Berlin, 2019; Vol. 1891, pp 247–255.
- (64) Winter, G. xia2: an expert system for macromolecular crystallography data reduction. *J. Appl. Crystallogr.* **2010**, *43*, 186–190.
- (65) Winn, M. D.; Ballard, C. C.; Cowtan, K. D.; Dodson, E. J.; Emsley, P.; Evans, P. R.; Keegan, R. M.; Krissinel, E. B.; Leslie, A. G. W.; McCoy, A.; McNicholas, S. J.; Murshudov, G. N.; Pannu, N. S.; Potterton, E. A.; Powell, H. R.; Read, R. J.; Vagin, A.; Wilson, K. S. Overview of the CCP4 suite and current developments. *Acta Crystallogr., Sect. D: Biol. Crystallogr.* **2011**, *67*, 235–242.
- (66) McCoy, A. J.; Grosse-Kunstleve, R. W.; Adams, P. D.; Winn, M. D.; Storoni, L. C.; Read, R. J. Phaser crystallographic software. *J. Appl. Crystallogr.* **2007**, *40*, 658–674.
- (67) Adams, P. D.; Afonine, P. V.; Bunkoczi, G.; Chen, V. B.; Davis, I. W.; Echols, N.; Headd, J. J.; Hung, L.-W.; Kapral, G. J.; Grosse-
- Kunstleve, R. W.; McCoy, A. J.; Moriarty, N. W.; Oeffner, R.; Read, R. J.; Richardson, D. C.; Richardson, J. S.; Terwilliger, T. C.; Zwart, P. H. PHENIX: a comprehensive Python-based system for macromolecular structure solution. *Acta Crystallogr., Sect. D: Biol. Crystallogr.* **2010**, *66*, 213–221.
- (68) Emsley, P.; Cowtan, K. Coot: model-building tools for molecular graphics. *Acta Crystallogr., Sect. D: Biol. Crystallogr.* **2004**, *60*, 2126–2132.
- (69) Davis, I. W.; Leaver-Fay, A.; Chen, V. B.; Block, J. N.; Kapral, G. J.; Wang, X.; Murray, L. W.; Arendall, W. B.; Snoeyink, J.; Richardson, J. S.; Richardson, D. C. MolProbity: all-atom contacts and structure validation for proteins and nucleic acids. *Nucleic Acids Res.* **2007**, *35*, W375–W383.